NREL/TP-411-5123 • UC Category: 271 • DE93000023

Electron Cyclotron Resonance Deposition of Amorphous Silicon Alloy Films and Devices

Final Subcontract Report 1 April 1991 – 31 March 1992

NREL/TP--411-5123

DE93 000023

Y.-H. Shing
Jet Propulsion Laboratory
Pasadena, California

NREL technical monitor: W. Luft

National Renewable Energy Laboratory
1617 Cole Boulevard
Golden, Colorado 80401-3393
A Division of Midwest Research Institute
Operated for the U.S. Department of Energy
under Contract No. DE-AC02-83CH10093

Prepared under Subcontract No. DD-1-11002-1

October 1992

On September 16, 1991 the Solar Energy Institute was designated a national laboratory, and its name was changed to the National Renewable Energy Laboratory.

Printed in the United States of America
Available from:
National Technical Information Service
U.S. Department of Commerce
5285 Port Royal Road
Springfield, VA 22161

Price: Microfiche A01
Printed Copy A04

Codes are used for pricing all publications. The code is determined by the number of pages in the publication. Information pertaining to the pricing codes can be found in the current issue of the following publications which are generally available in most libraries: *Energy Research Abstracts (ERA)*; *Government Reports Announcements* and Index (*GRA* and I); *Scientific and Technical Abstract Reports (STAR)*; and publication NTIS-PR-360 available from NTIS at the above address.

PREFACE

This report was prepared as an account of work sponsored by an agency of the United States Government. Neither the United States Government nor any agency thereof, nor any of their employees makes any warranty, expressed or implied, or assumes any legal liability or responsibility for the accuracy, completeness, or usefulness of any information, apparatus, product, or process disclosed, or represents that its use would not infringe privately owned rights.

Reference herein to any specific commercial product, process, or service by trade name, trademark, manufacturer, or otherwise, does not necessarily constitute or imply its endorsement, recommendation, or favoring by the United States Government or any agency thereof. The views and opinions of authors expressed herein do not necessarily state or reflect those of the United States Government or any agency thereof.

This document reports on work done under NASA Task RE-152, Amendment No. 481.

EXECUTIVE SUMMARY

The advantages of electron cyclotron resonance (ECR)-microwave plasma-enhanced chemical deposition (PECVD) include: separate control of plasma chemistry and film deposition mechanisms; reduced substrate temperatures; enhanced deposition rates; high plasma densities; enhanced plasma ionization ratios; and low, controllable and selective ion energies incident upon the growth surface. These provide very desirable processing conditions for modifying film growth kinetics and for enhancing the surface reactions which promote growth at reduced substrate temperatures.

The objective of this work was to obtain a fundamental understanding of amorphous silicon (a-Si:H) and related alloy thin film deposition processes by ECR microwave plasmas, with a best effort improvement of optoelectronic material properties and best effort photostabilization of solar cell performance. The Jet Propulsion Laboratory (JPL) developed a state-of-the-art ECR PECVD system for the deposition of a-Si:H and related alloy thin films.

We systematically and extensively investigated the ECR deposition parameter space for a-Si:H. Materials characterization included constant photocurrent measurement (CPM), to determine the Urbach slopes; junction capacitance measurements and drive-level capacitance profiling (DLCP), to determine the total integrated densities of filled defect states; optical transmission measurements, to determine the optical band gaps; light and dark photoconductivity measurements, to determine the photosensitivities; and small angle x-ray scattering (SAXS) measurements, to determine the microvoid fractions and distributions.

We fabricated and tested diagnostic solar cells in order to provide device evaluations of the thin films. The ECR-deposited p-type a-SiC:H and intrinsic a-Si:H films, which were of primary interest to solar cells, underwent individual evaluation under device conditions as components of p-i-n solar cells with standard radio-frequency (RF) films for the remaining layers. This required physical transfer of samples between the ECR and RF chambers, exposing the samples to air between layers and leading to some degradation of the interfaces. We obtained initial efficiencies as high as 5.9% for cells containing ECR p-type a-SiC:H windows, and initial efficiencies as high as 2.9% for cells containing ECR intrinsic layers. We emphasize that this low performance appears to be caused primarily by the interface degradation and does not appear to be related to ECR materials deficiencies. In support of this, RF-deposited cells with air exposure of the interfaces showed similarly degraded performance, from 7.7% for unexposed to 3.6% for exposed interfaces. Also, light-soaked ECR a-Si:H showed an increase in defect density, measured via junction capacitances, which was comparable to that of analogous RF-deposited a-Si:H.

Finally, we compared conventional ECR-deposited a-Si:H to a new form of a-Si in which xenon gas was added to the ECR plasma during deposition. The new films, termed a-Si:(Xe,H), possessed low, stable dark conductivities and high photosensitivities. Light soaking experiments revealed photodegradation rates which were about 35% less than those of comparable RF-deposited material. Diagnostic solar cells containing a-Si:(Xe,H) i-layers, with air-exposed p/i and i/n interfaces, showed modest initial efficiencies of 4.1%. In perspective, a corresponding RF-deposited cell with air-exposed interfaces had an identical conversion efficiency of 4.1%. Again, this low performance appears to be caused primarily to the interface degradation and does not appear to be related to ECR materials deficiencies.

Work on both ECR a-Si:H and a-Si:(Xe,H) could not proceed further under this task because of its termination. Although ECR material, particularly a-Si:(Xe,H) shows much promise in terms of materials photostability, we cannot yet make a solid assessment of device performance and stability cannot yet be made, partially because photostability is not necessarily related to device stability.

CONTENTS

FIGURE CAPTIONS

LIST OF TABLES

A. INTRODUCTION AND BACKGROUND

Electron cyclotron resonance (ECR) microwave plasma enhanced chemical vapor deposition (PECVD) had generated a great deal of interest in the mid to late 1980's for deposition of a-Si:H and related binary alloy thin films. The ECR PECVD is a remote plasma deposition technique which separates the plasma generation from the film deposition. Hence, plasma chemistry and film deposition mechanisms can be separately controlled in the ECR PECVD. This provides an additional degree of freedom for controlling the material properties in the ECR deposition process. Advantages that have been identified with the ECR microwave plasma deposition method for device applications are reduced substrate temperatures, enhanced deposition rates and effective control over low energy ions incident on the growth surface.

ECR microwave plasmas are typically produced at low gas pressures (10^{-4} to 10^{-2} Torr), with a high plasma density ($10^{11}/cm^3$ and a high ionization ratio (10^{-2}). The corresponding values for RF plasmas are $10^9/cm^3$ and 10^{-5}, respectively. These ECR plasma characteristics are the key features which can be exploited to develop a controllable thin film deposition process. In addition, the ion energy of ECR plasmas is in the low tens of electron volts, compared with hundreds of electron volts in RF plasmas, because of the moderate sheath voltages of the microwave excitation. The low ion energy of ECR plasmas can be selected and controlled in the range of 5 ~100 Ev by remote extraction with a divergent or mirror magnetic field and an applied RF basis to the substrate stage. The high plasma density, enhanced ionization ratio, and well-defined, low ion energy in the ECR plasma provide very desirable processing conditions for modifying film growth kinetics and for enhancing the surface reactions which promote growth at lower substrate temperatures.

Although the above-mentioned special features of ECR plasmas are highly desirable in thin film deposition technology, ECR PECVD has a more complex deposition parameter space than conventional RF PECVD. Additional deposition parameters, such as microwave excitation mode, magnetic field profile and substrate bias, are involved in the ECR process. These additional parameters may play important roles in determining the optoelectronic and structural properties of the ECR-deposited films. In order to fully realize the advantages of the ECR deposition process, the complex deposition parameter space has to be extensively investigated.

The objective of this research project was to obtain an understanding of amorphous silicon (a-Si:H) and related alloy thin film deposition processes by ECR microwave plasmas, with a best effort improvement of optoelectronic material properties and best effort photostabilization of solar cell device performance.

JPL developed a state-of-the-art ECR microwave (2.45 Ghz) PECVD system for the deposition of a-Si:H and related alloy thin films. The ECR deposition parameter space of a-Si:H films was systematically investigated. Using ECR microwave plasmas with silane and hydrogen gas mixtures, we deposited photosensitive, device-quality a-Si:H films. Materials characterization of ECR-deposited a-Si:H films included the constant photocurrent method (CPM), to determine the Urbach slopes; junction capacitance measurements, to determine the defect densities; drive-level capacitance profiling (DLCP), to determine the total integrated densities of filled defect states; optical transmission measurements, to determine the optical band gaps; small-angle x-ray scattering (SAXS) measurements, to determine the microvoid fractions and distributions; and light and dark conductivity measurements, to determine the photosensitivities. We fabricated diagnostic solar cells containing ECR-deposited p-type a-Si:H and intrinsic a-Si:H layers to provide device evaluations of these films.

Finally, we developed a novel method of depositing a-Si:H films developed using xenon, hydrogen and silane mixed gas ECR plasmas. These Xe ECR plasmas deposited a-Si:(Xe,H) films showed very promising material properties pointing towards improved photostability. Initial characterization of ECR-deposited a-Si:(Xe,H) films focused upon Fourier transform infrared spectroscopy (FTIR), CPM, SAXS and conductivity measurements. Diagnostic solar cells containing ECR-deposited a-Si:(Xe,H) films were also fabricated. However, it should be noted that the early termination of this research project prevented a complete assessment of the material properties and device potential of this new type of ECR-deposited a-Si.

B. EXPERIMENTAL

The ECR microwave plasma depositions of a-Si:H and a-SiC:H films were performed using SiH_4, CH_4 and H_2 gas mixtures. The ECR microwave PECVD system consists of an ECR ion source and a deposition chamber equipped with an RF induction heated sample stage. The ECR plasma is generated by microwave (2.45 GHz) power and a resonant (875 Gauss) magnetic field in a cylindrical plasma chamber. The microwave power is transmitted in a rectangular waveguide and is coupled to the plasma chamber via a symmetrical mode coupler and a quartz window. The ECR resonant condition is set up at the upper portion of the plasma chamber by one magnet; a divergent, mirror magnetic field profile is set up by another magnet to extract the ECR plasma into the deposition chamber. The plasma gas, such as H_2, is introduced at the top of the plasma chamber; the source gases, such as SiH_4 and CH_4, are injected into the deposition chamber. The sample stage is mounted on a 20" stem which allows the substrates to be located at a distance of 5" below to 12" above the aperture of the plasma chamber. The sample stage can be RF induction heated to a maximum temperature of 1000°C using a 3.75 kW, 60 kHz RF power supply. A high frequency (13.56 MHz) RF bias can be applied to the substrate stage which is electrically isolated from the system ground. A schematic diagram of the ECR deposition system is shown in Figure 1.

The conductivity measurements of ECR-deposited a-Si:H films were performed using two parallel electrodes of evaporated silver with a planar geometry of 1 cm length and 1 mm separation. Light conductivities were measured under 100 mW/cm^2 mercury lamp illumination. The photosensitivity, defined as the light-to-dark conductivity ratio, was employed as a film quality indicator.

Constant photocurrent and junction capacitance measurements, as well as drive-level-capacitance profiling (DLCP), were performed on JPL-prepared samples in collaboration with J. Essick of Occidental College. ECR a-Si:H films deposited on Corning 7059 glass substrates were evaluated for constant photocurrent measurements. Sample geometry consisted of two planar parallel evaporated silver electrodes, 1 cm in length and separated by 1 mm. Each sample configuration for junction capacitance measurements consisted of 1 to 2 μm thick, ECR-deposited a-Si:H films on crystalline silicon substrates. A Schottky barrier was formed by depositing a Pd on Cr contact (area = 20 mm^2) onto the a-Si:H.

The illuminated current-voltage characteristics of a-Si:H solar cells were measured by using a Spectrolab XT-10 solar simulator. The light intensity of the solar simulator was calibrated to 100 mW/cm^2 by using a Schott color glass (KG5) filtered silicon reference cell (sample number S23) provided by NREL. The reference spectral response was as anticipated for a-Si:H. The efficiency of the cell was 5.3% under these conditions.

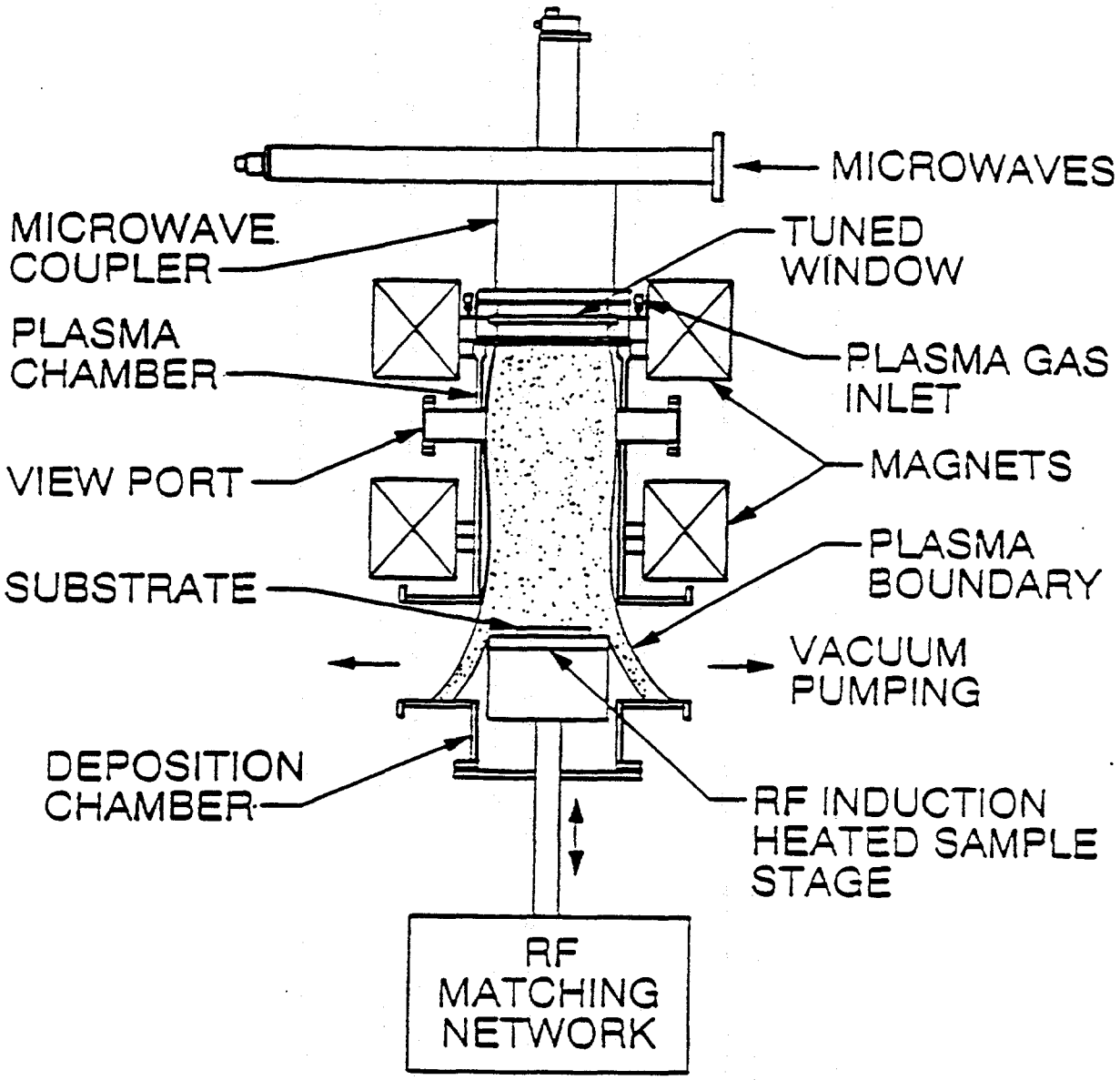

Figure 1. Schematic Diagram of the ECR Deposition System

C. RESULTS AND DISCUSSION

1. Material Properties of ECR-Deposited a-Si:H Films

We optimized the ECR deposition process for photosensitive a-Si:H films by systematically investigating the parameter space of substrate temperature and mirror magnetic field profile. We varied the substrate temperature over the temperature range of 100°C to 300°C. We generated the ECR plasmas under identical conditions for all depositions, using a microwave power of 300 W and deposition pressure of 4 mTorr. We positioned the ECR resonant magnetic field of 875 Gauss directly below the quartz window of the plasma chamber and set the mirror magnetic field at 375 Gauss. We used a gas mixture of SiH_4 and H_2 as the deposition source with flow rates of 15 and 45 cm/sec, respectively.

The deep defect density is interpreted as a direct measure of the density of dangling bonds and hence, is essential information in evaluating the quality of a-Si:H films. We obtained the total integrated density of filled deep defect states through drive-level-capacitance profiling (DLCP). This technique yields the integrated density of filled gap states for differing "slices" of the density of states (DOS), evaluated from E_c-E_f down to a thermal escape depth $E_c-E_e = kT \ln(\omega/\nu_0)$, where T and ω are the measurement temperature and frequency, respectively and ν_0 is the thermal emission prefactor. By adjustment of the sample temperature, different sections of the density of states may be profiled. Thus, at 1 Hz, assuming a value of $\nu_0 = 10^{13}$ s^{-1}, the DOS is probed to E_c-E_e = 0.775, 0.823, 0.872, 0.920 and 0.968 Ev at T = 320, 340, 360, 380 and 400 K, respectively.

Figure 2 displays typical C-T data taken on a sample at frequencies of 1, 10 and 100 Hz. Values for ν_0 from the Arrenhius plots were in the expected range of 10^{12}-10^{13} s^{-1}. The temperature dependence of the Fermi level is given in Figure 3, which shows a deepening of the Fermi level with increasing deposition temperature. We used the activated (high-temperature) capacitance values in the DOS modelling, as discussed below.

We used a 1-Hz CPM measurement to determine the Urbach slopes. Figure 4 shows the Urbach slope as a function of deposition temperature. For temperatures of 175-250°C, we observed Urbach slopes in the 50-60 meV range, indicative of device-quality a-Si:H. We analyzed optical transmission data to obtain Tauc plots, from which we determined the optical gaps. The optical gap as a function of temperature is given in Figure 5. This shows a decrease in the gap with increasing temperature which closely resembles that for RF glow-discharge a-Si:H films, although shifted to a wider gap by approximately 0.1 eV.

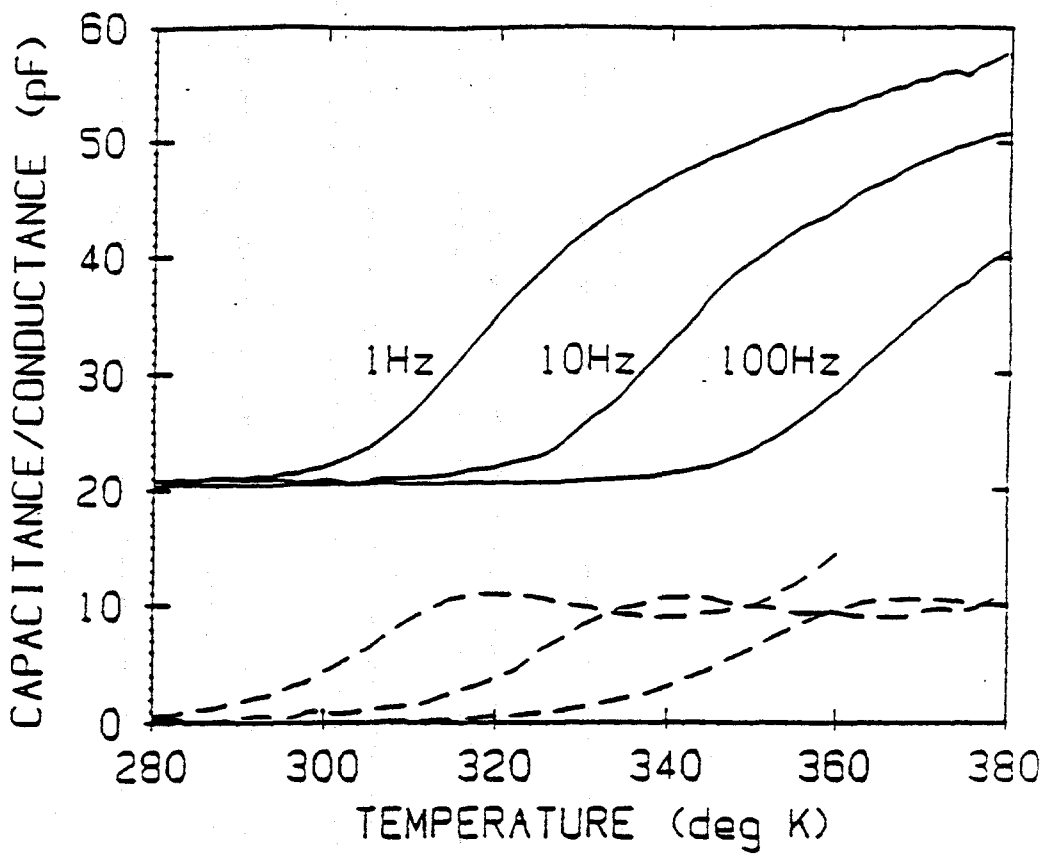

Figure 2. Typical capacitance (solid line) and conductance divided by angular frequency (dashed lines) vs. temperature at -2V bias for three measurement frequencies. ECR film was deposited at 175°C. Arrenhius plot slope gives E_t = 0.75eV.

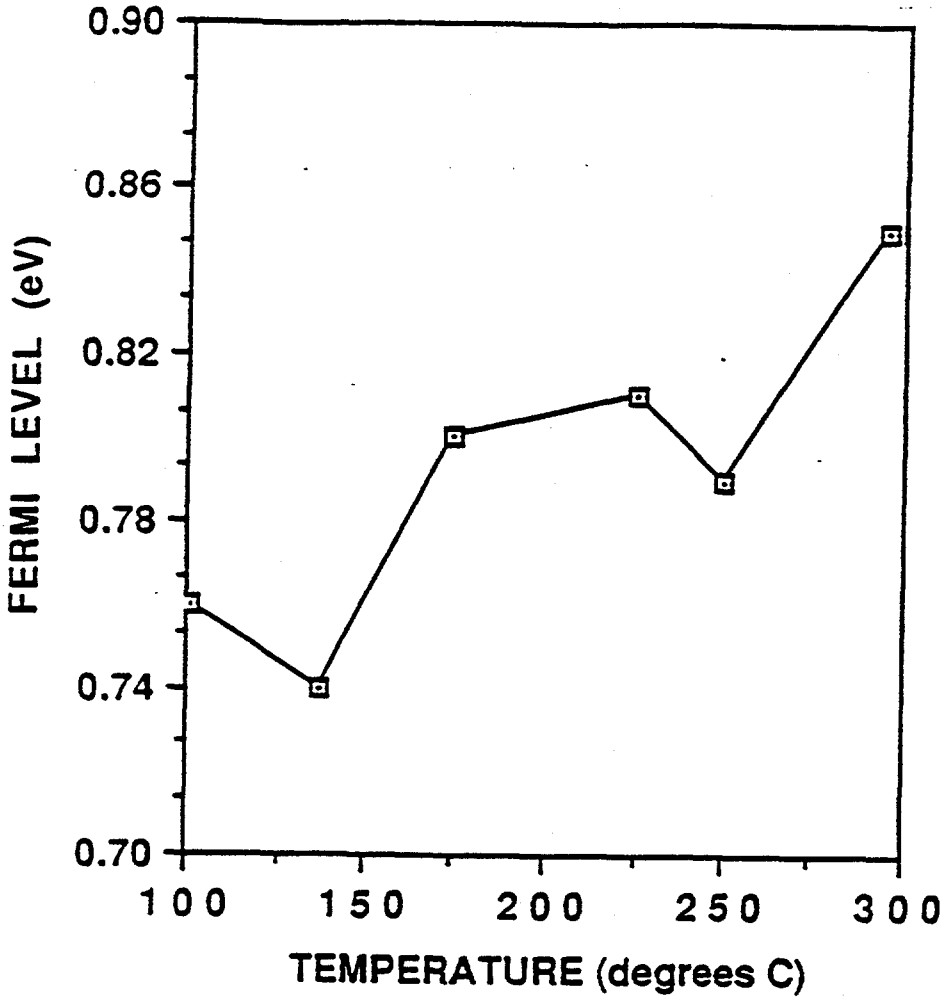

Figure 3. Fermi level position of ECR-deposited, photosensitive a-Si:H films as a function of deposition temperature.

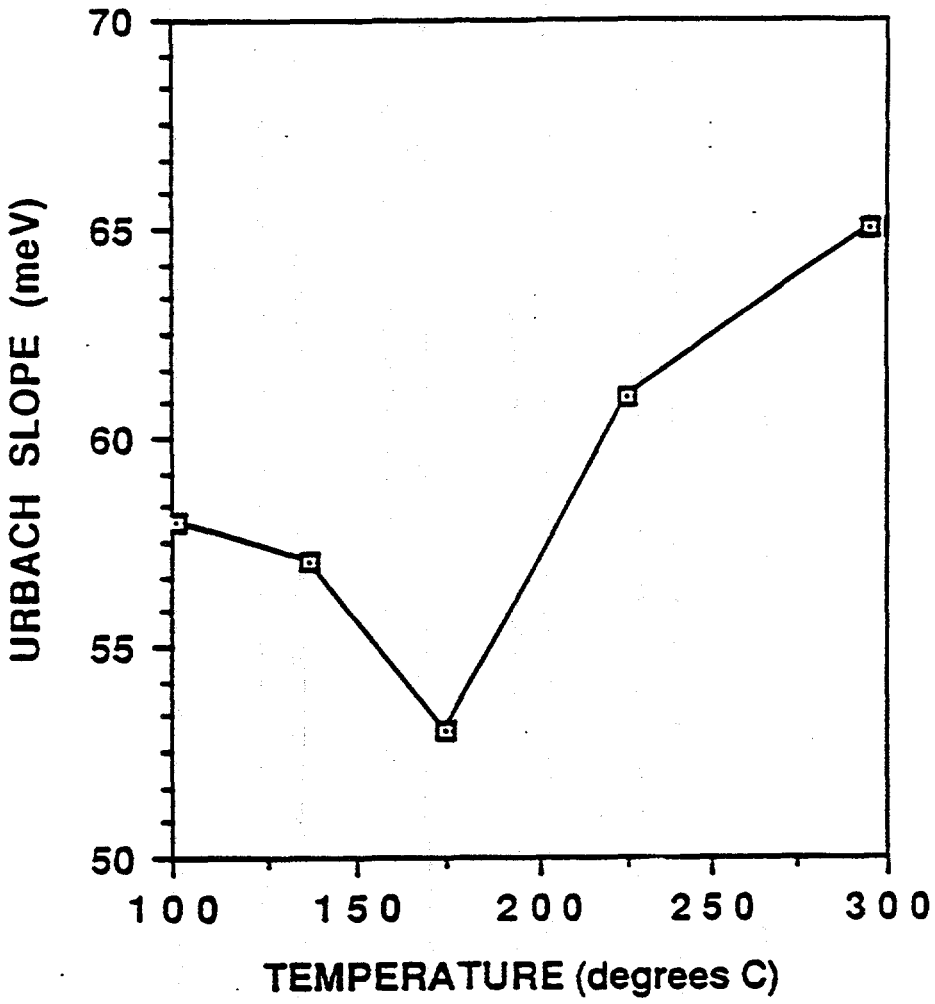

Figure 4. Urbach slopes of ECR-deposited, photosensitive a-Si:H films as a function of deposition temperature

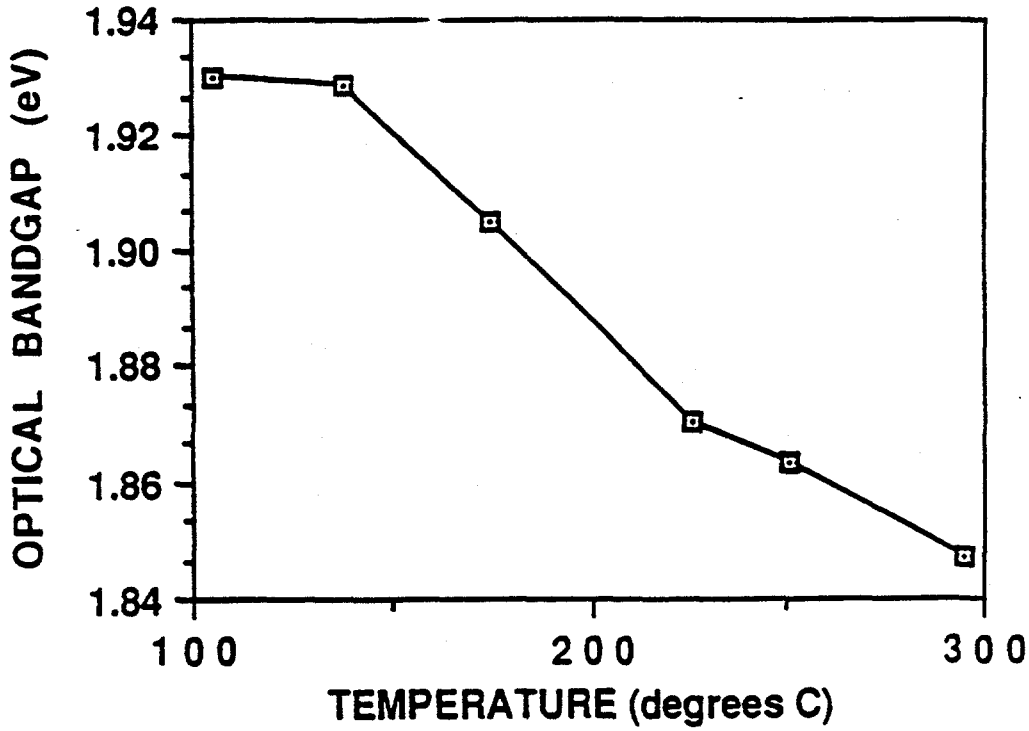

Figure 5. Optical gap as a function of deposition temperature.

We determined the total integrated density of deep defect states for each ECR deposited sample by model calculations. We assumed that the DOS spectrum for those samples consisted of two Gaussian (σ=0.15 eV) subbands centered at E_c-0.6 eV and E_c-0.9 eV and a 25 meV exponential conduction-band tail. By assuming these subbands, variation of defect widths and positions over a range consistent with previously reported value resulted in less than a 10% variation in the modeled defect densities. By appropriate choice of magnitude for each subband, we replicated the drive-level data for a given ECR sample for each measurement temperature (i.e., E_c-E_f). For a given applied bias, we next determined the resulting band bending produced by this assumed DOS then was determined by numerically solving Poisson's equation. In turn, we used this solution to predict the activated capacitance values, which we compared to those actually observed in the C-T data. After several iterations of this process, we determined each sample's DOS, yielding a value for its integrated density of filled deep defects. Typically, this procedure yielded a modeled deep defect density equal to 2.5-3.0 times the highest-temperature drive-level density, indicating that approximately one-third of the deep defects are above midgap. Figure 6 shows the integrated density of filled deep defects as a function of deposition temperature. As can be seen, depositions from ECR plasmas in the 175-300°C temperature regime resulted in high-quality a-Si:H with 1-2x10^{16} cm^{-3} deep defects. In comparing the temperature dependence of the defect density for ECR grown a-Si:H to identical studies for glow-discharge a-Si:H, both systems are found to exhibit very similar behavior.

We performed light soaking of ECR-deposited a-Si:H films under concentrated AM 1.5 simulated solar illumination with a concentration ratio of 10 at 50°C for 12 hours, which is equivalent to one sun AM 1.5 illumination time for about 750 hours. We determined the integrated defect density by junction capacitance measurements for the initial and the light-soaked states. Table I lists the Fermi levels and the defect densities of initial and light-soaked states of a-Si:H films deposited under various conditions. The defect density of the light-soaked state was increased by a factor of about 3 to 3.5, as compared to the initial defect density. This factor of increase of the light-soaked defect density for ECR-deposited a-Si:H films is similar to that of RF-deposited, device-quality a-Si:H films.

S. Jones and D. Williamson of the Colorado School of Mines performed small angle x-ray scattering (SAXS) measurements on ECR-deposited a-Si:H films. We prepared six samples for SAXS measurements by using special aluminum foil substrates. Drs. Jones and Williamson determined that the spherical void fraction for these ECR-deposited a-Si:H films ranged between 4.8% and 8.5%. The void size distribution of an ECR-deposited a-Si:H film with a void fraction of 4.8% is shown in Figure 7. The distribution of voids in this film is dominated by 50% small voids, with an average diameter of 0.9μm. For comparison purposes, the spherical void

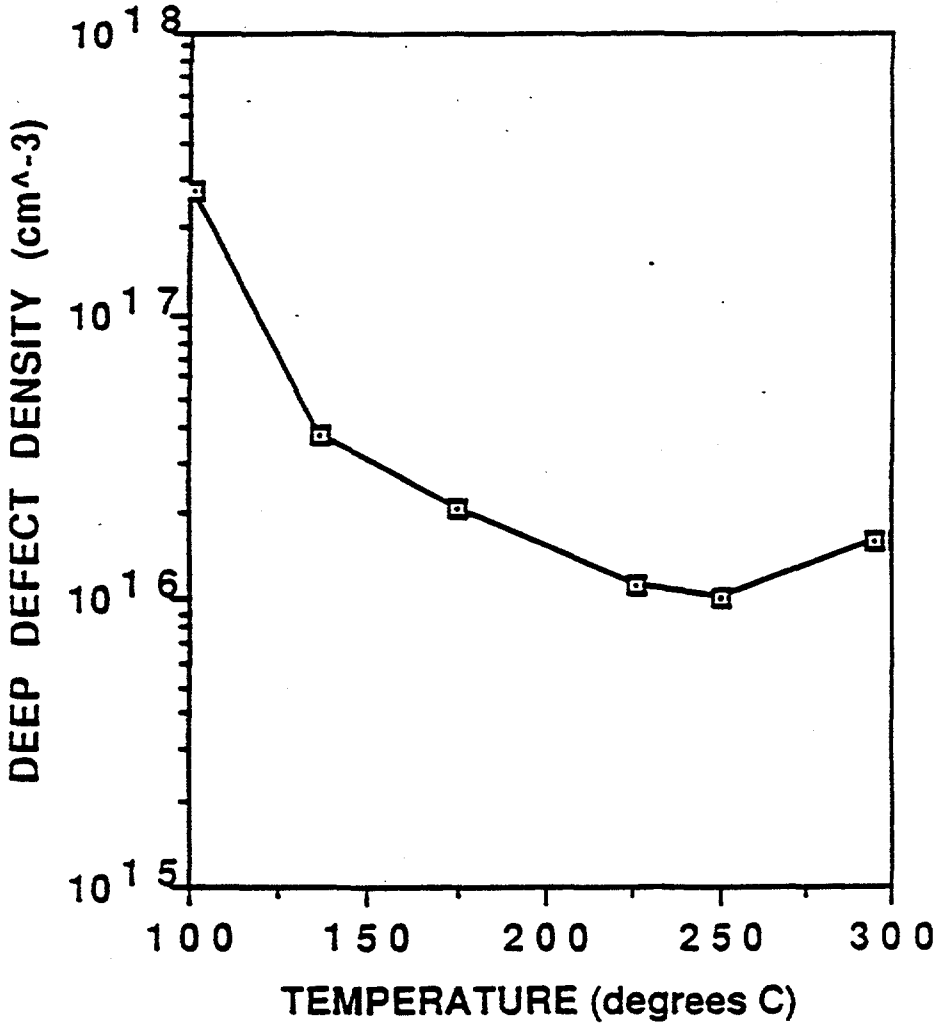

Figure 6. Integrated filled deep defects of ECR-deposited, photosensitive a-Si:H films as a function of deposition temperature.

Table I.

Initial and Light-Soaked Defect Density of ECR-Deposited a-Si:H Films

SAMPLE NUMBER	10613C	10520B	01207C
Initial Defect Density N_D^A (cm^{-3})	1.5×10^{16}	1.8×10^{16}	4.5×10^{15}
Light-Soaked Defect Density N_D^B (cm^{-3})	4.8×10^{16}	6.6×10^{16}	1.5×10^{16}
Defect Density Ratio N_D^B/N_D^A	3.2	3.7	3.3
Initial Fermi Level E_f^A (eV)	0.82	0.83	0.87
Light-Soaked Fermi Level E_f^B (eV)	0.79	0.80	0.75
Deposition Pressure (mTorr)	0.6	0.6	4
Substrate Temperature (°C)	200	200	175

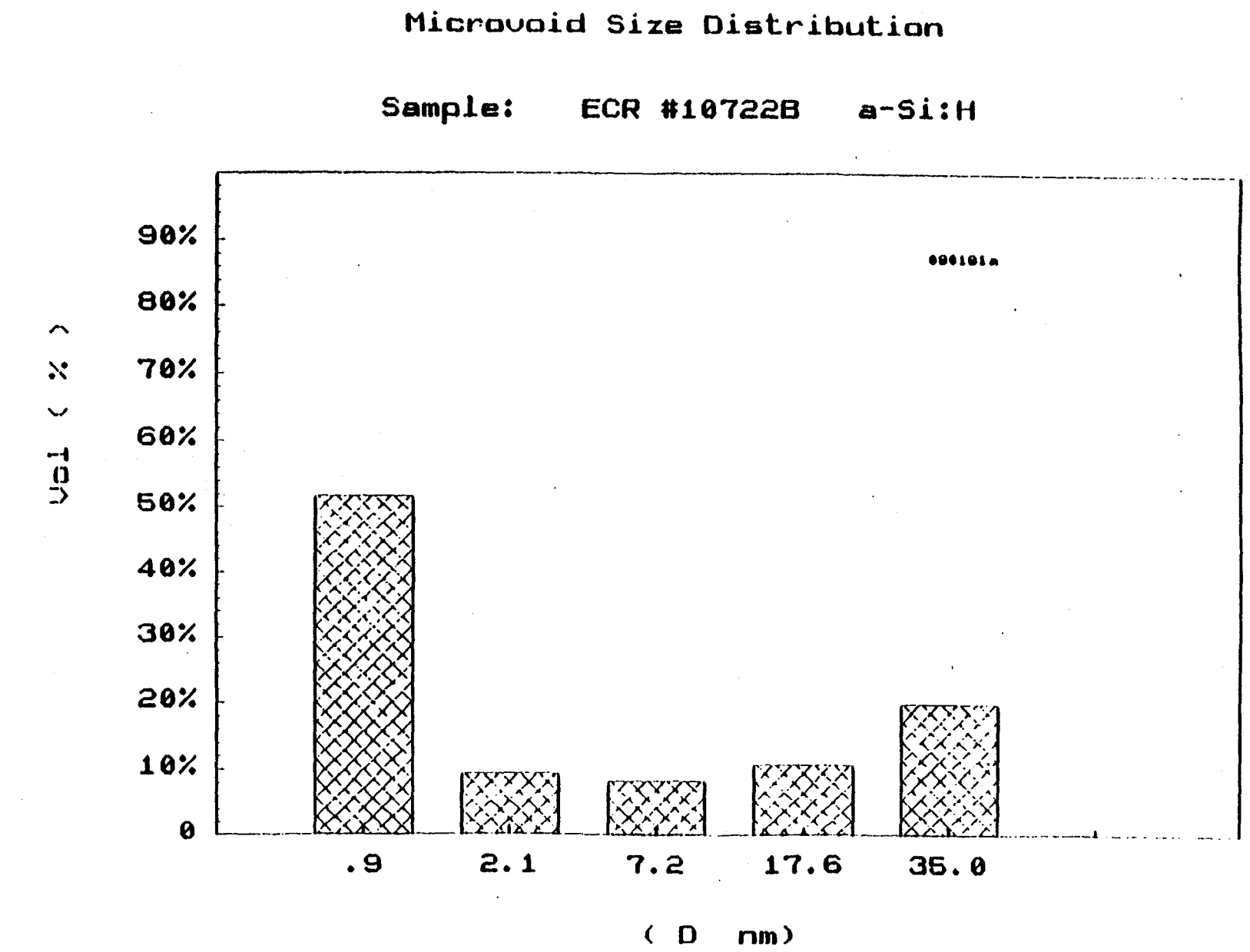

Figure 7. Microvoid distribution of an ECR-deposited a-Si:H film as determined by SAXS measurements.

fraction of device-quality, RF-deposited a-Si:H films is lower, 0.5% to 1%; and the RF void size distribution is dominated by a larger fraction (80%) of small voids. The void characteristics of ECR-deposited a-Si:H films should next be correlated with the optical and electronic properties of these films and their deposition conditions.

2. The Effect of the Magnetic Field Profile Upon the ECR Deposition Process

The energy of ions in the plasma stream extracted from the ECR plasma chamber into the deposition chamber depends upon the magnetic field profile. A systematic variation of the magnetic field profile can provide an additional control of the film quality in the ECR deposition process. Figure 8 shows a set of magnetic field profiles as a function of the distance from the quartz window. We set the ECR resonant condition at the quartz window; and we set the mirror magnetic field at 13" from the quartz window with various strengths from 100-850 Gauss. Using this set of magnetic field profiles, we deposited a-Si:H films under 0.6 mTorr pressure, 300 W microwave power, 200°C substrate temperature, 30 sccm H_2 flow rate and 10 sccm SiH_4 flow rate. The Urbach slope and the integrated defect density of these a-Si:H films as a function of the mirror magnetic field strength are shown in Figures 9 and 10, respectively. The mirror magnetic field dependence indicates that the Urbach slope and the defect density are optimized in the mirror magnetic field range of 300-700 Gauss. The optimized film quality probably results from the mirror magnetic field selection of ions with proper energies incident on the film growth surface.

We next analyzed the ion density of ECR microwave plasmas with Langmuir probe measurements. We measured the ion current with a cylindrical tungsten Langmuir probe at the position of film growth while altering the mirror magnetic field profile. Figures 11 and 12 show the correlation between the deposition rate and the ion density as a function of the mirror magnetic field at deposition pressures of 5 mTorr and 0.7 mTorr, respectively. The direct correlation shown in Figure 11 indicates that the film growth at 5 mTorr is dominant by the plasma deposition process related to the electron impact dissociation of silane. However, the apparent anti-correlation shown in Figure 12 is probably the result of significant plasma etching produced at low pressures. The increase of the ion density at low mirror magnetic fields may have caused excessive plasma etching or sputtering due to the increase of ion energies at low pressures.

The correlations between the defect density and the ion current as a function of the mirror magnetic field are shown in Figures 13 and 14 for deposition pressures at 5 mTorr and 0.7 mTorr, respectively. The direct correlation shown in Figure 13 is consistent with the plasma etching or sputtering at low pressures, caused by high-energy ions which can also generate defects resulting in an increase of the defect density. The anti-correlation between the defect density and the ion density at low mirror magnetic fields shown in Figure 14 indicates that there is a threshold in the ion density and the ion energy for producing an optimized defect density. These correlation studies on the deposition rate, defect density and ion density show that the ECR deposition process can be sensitively controlled by varying the ion density and energy.

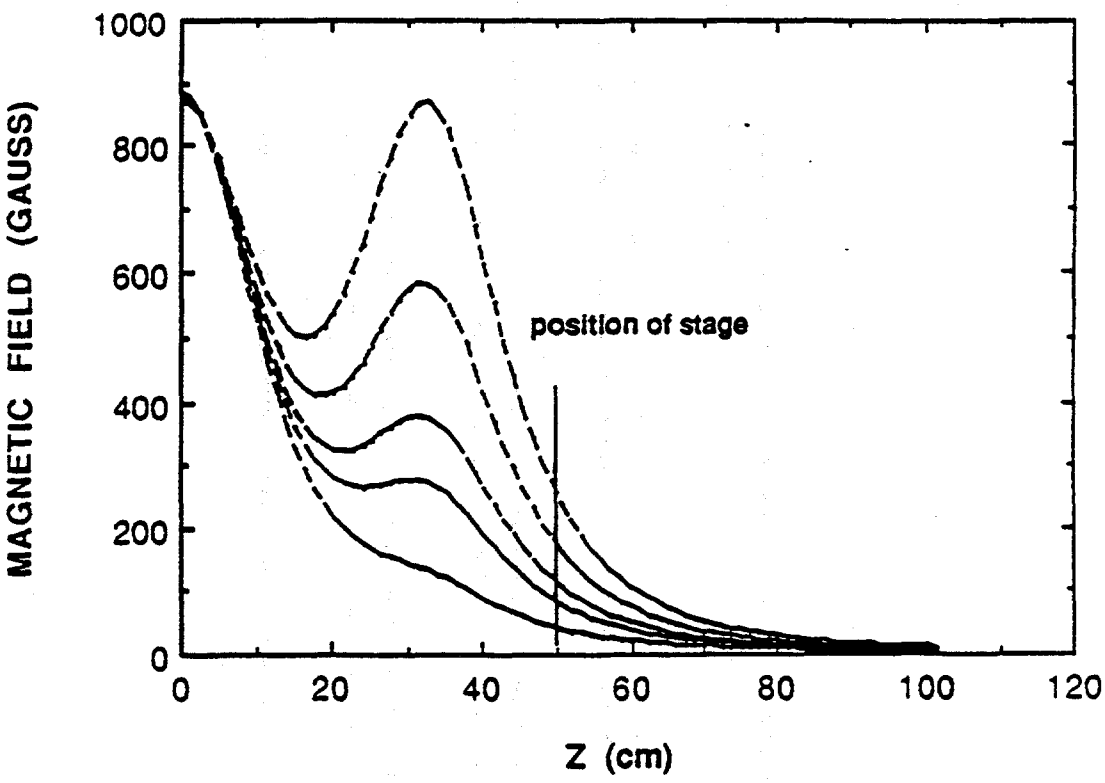

Figure 8. Mirror magnetic profiles used in ECR depositions of photosensitive a-Si:H films.

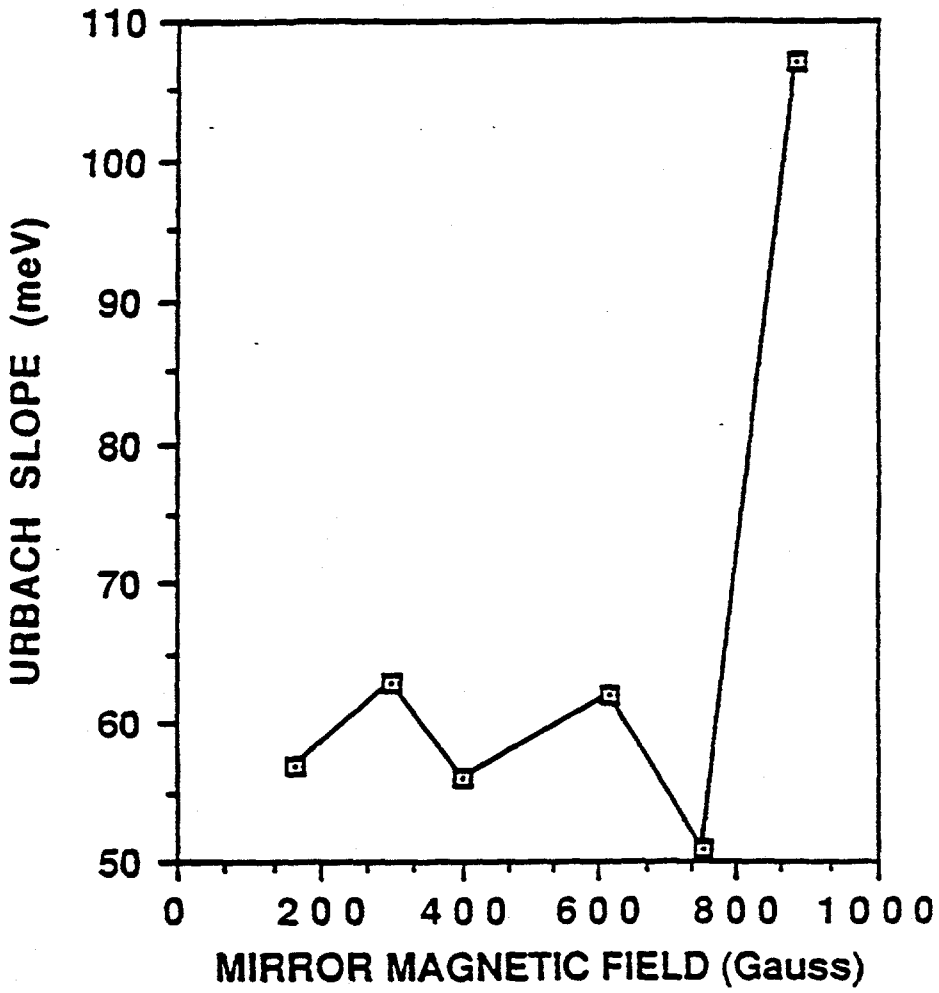

Figure 9. Urbach slope of ECR-deposited, photosensitive a-Si:H films as a function of mirror magnetic field strength.

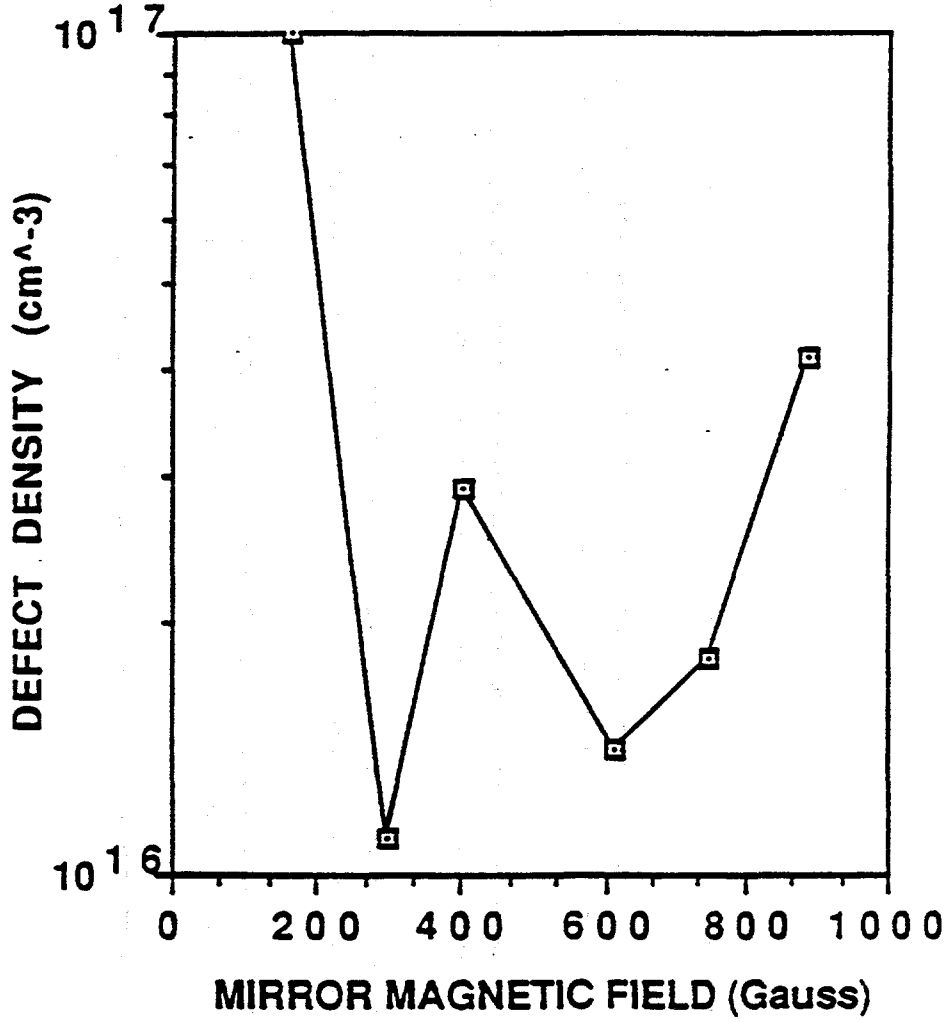

Figure 10. Integrated deep defect density of ECR-deposited, photosensitive a-Si:H films as a function of mirror magnetic field strength.

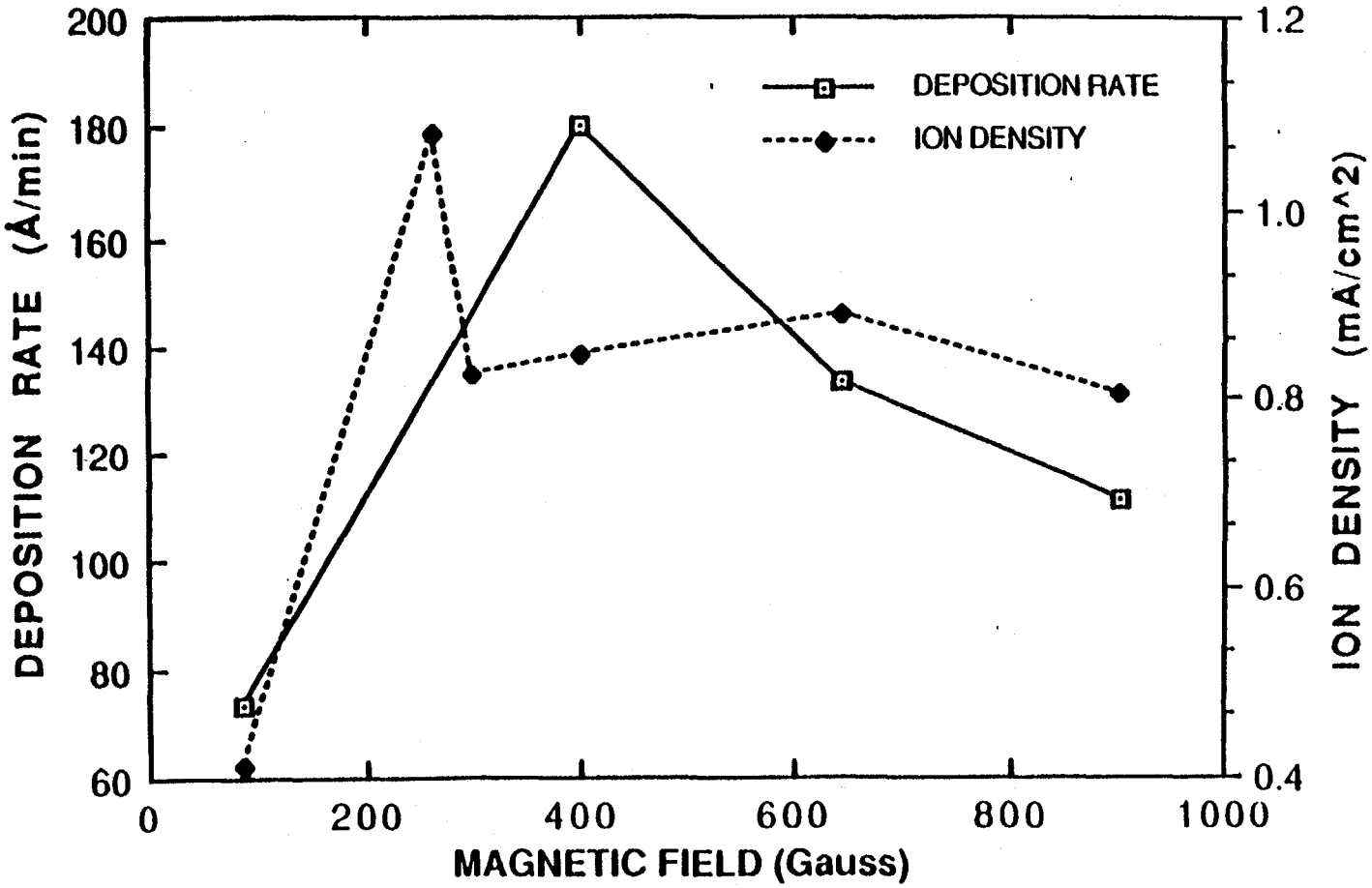

Figure 11. Deposition rate and ion density as a function of mirror magnetic field for ECR deposition under 5 mTorr pressure.

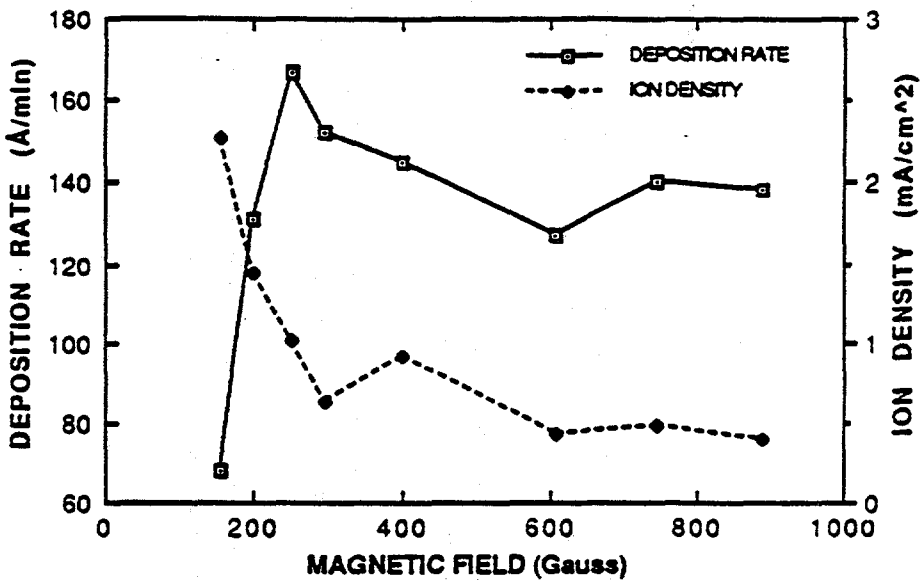

Figure 12. Deposition rate and ion density as a function of mirror magnetic field for ECR deposition under 0.7 mTorr pressure.

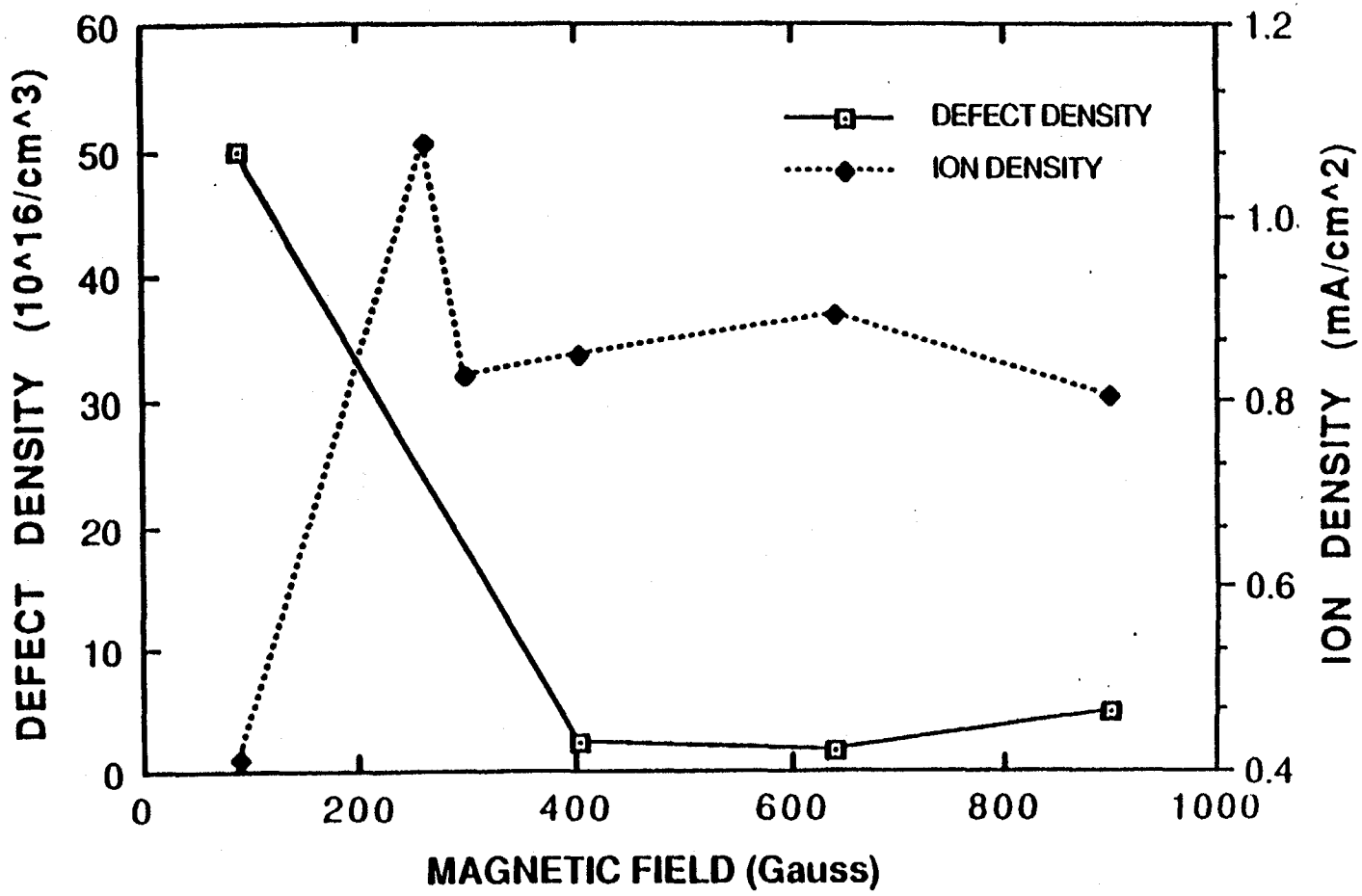

Figure 13. Defect density and ion density as a faunction of mirror magnetic field for ECR deposition udner 5 mTorr pressure.

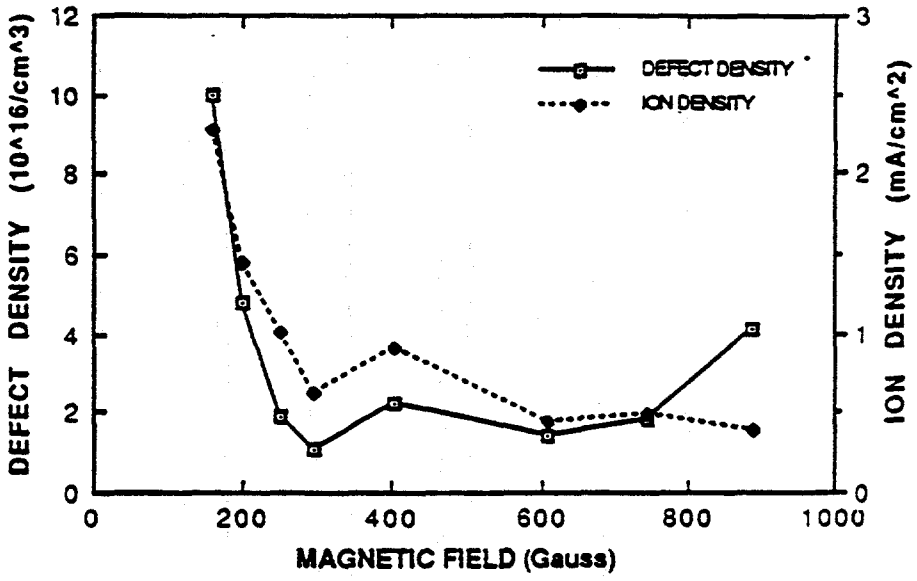

Figure 14. Defect density and ion density as a function of mirror magnetic field for ECR deposition under 0.7 mTorr pressure.

3. Evaluation of ECR-Deposited p-type a-SiC:H and Intrinsic a-Si:H Films Using Diagnostic p-i-n Solar Cells

We individually evaluated ECR-deposited p-type a-SiC:H and intrinsic a-Si:H films, which are of primary device interest, by fabricating p-i-n solar cells with standard RF-deposited films for the remaining layers. To evaluate ECR-deposited p-type a-SIC:H window layers, we employed RF-deposited i and n layers to complete the solar cell structure. Likewise, we evaluated ECR-deposited intrinsic a-Si:H films by fabricating the p-i-n diagnostic device with RF-deposited p and n layers. Due to the transfer of samples between the ECR and RF deposition systems, the interface between the p and i and between the i and n layers were exposed to air during the fabrication of devices containing an ECR-deposited i-layer. Air exposure of the interfaces in the fabrication of diagnostic solar cells is a major uncontrolled factor in comparing the performance of the diagnostic and the standard (RF-deposited) p-i-n solar cells. In future work, an addition of an interlock between the two chambers would be one prospective solution to this problem.

Table II lists the fabrication conditions and performances of diagnostic solar cells containing ECR-deposited p-type and intrinsic layers. We used textured SnO_2 coated 7059 glasses, provided by Solarex Thin Film Division, and specular SnO_2 coated soda lime glasses, purchased from Nippon Sheet Glass (NSG) Company as substrates for fabricating p-i-n solar cells. Diagnostic solar cells incorporating an ECR-deposited p-type a-SiC:H window layer have shown efficiencies of 5.9%. Air exposure of the p/i interface in these diagnostic solar cells is probably the major cause of the reduction of the short-circuit current (J_{sc}) from the standard 14.7 mA/cm^2 to the observed 12.9 mA/cm^2. Diagnostic solar cells showed severe degradation of J_{sc} and fill factor to 7.45 mA/cm^2 and 46.4%, respectively. It is emphasized that this severe degradation is most likely caused by the air exposure of both the p/i and i/n interfaces, and does not appear to be related to ECR materials deficiencies.

We also fabricated standard p-i-n a-Si:H solar cells using the RF glow discharge deposition process. We previously developed baseline RF deposition processes for intrinsic, p-type and n-type a-Si:H films. The RF-deposited, device-quality intrinsic a-Si:H films showed light conductivities of about $1 \times 10^{-4} (\Omega\text{-cm})^{-1}$ and photosensitivities of about 10^5. The RF-deposited p-type a:SiC:H and n-type a-Si:H films showed conductivities of 2×10^{-5} and 2×10^{-4} $(\Omega\text{-cm})^{-1}$, respectively. An initial fabrication run of RF-deposited a-Si:H p-i-n baseline solar cells produced initial conversion efficiencies of 6.5%.

Table II.

CHARACTERISTICS OF DIAGNOSTIC SOLAR CELLS CONTAINING ECR-DEPOSITED LAYERS

CELL AREA (cm^2)	SUBSTRATE	DEPOSITION METHOD p	i	n	INTERFACIAL CONDITION p/i	i/n	V_{oc} (mV)	I_{sc} (mA/cm^2)	F.F.	INITIAL EFFICIENCY (%)
0.126	Textured SnO_2	ECR	RF	RF	Air	Vacuum	759	12.9	60.2	5.88
0.1	Specular SnO_2	ECR	RF	RF	Air	Vacuum	745	11.9	60.9	5.38
0.126	Textured SnO_2	RF	ECR	RF	Air	Air	841	7.45	46.6	2.92
0.1	Textured SnO_2	RF	ECR	RF	Air	Air	871	7.10	38.4	2.38
0.1	Textured SnO_2	RF	ECR	RF	Air	Air	841	5.63	42.5	2.01
0.1	Textured SnO_2	RF	RF	RF	Vacuum	Vacuum	869	14.7	60.4	7.69
0.1	Specular SnO_2	RF	RF	RF	Vacuum	Vacuum	875	13.0	64.0	7.26
0.1	Textured SnO_2	RF	RF	RF	Air	Air	1016	8.94	39.4	3.58
0.2	Textured SnO_2	RF	RF	RF	Vacuum	Air	920	10.4	36.8	3.51

We subsequently improved the performance of RF-deposited baseline a-Si:H solar cells by lowering the deposition temperature from 240° to 210°C. Figures 15 and 16 show the illuminated current-voltage characteristics of the improved RF baseline solar cells using Solarex and NSG SnO_2 coated glass substrates, respectively. Lowering of the deposition temperature improved V_{oc} from 735 mV to 869 mV, which raised the initial efficiency to 7.7%. The Solarex substrate with textured SnO_2 showed a Jsc of 14.7 mA/cm^2, which is about 20% higher than that of the NSG substrate with specular SnO_2.

The detrimental effects of exposing the p/i and i/n interfaces to air were also evident in standard RF-deposited p-i-n solar cells. The RF-deposited solar cells with air exposure of the p/i and i/n interfaces of only the i/n interface showed degradations of J_{sc} and fill factor similar to those of the diagnostic solar cells, reducing their initial conversion efficiencies from 7.7% to about 3.6%. Hence, the poor performance of the diagnostic solar cells can be attributed to air exposure of the interfaces. We also investigated several interfacial modification techniques, such as a hydrogen etch and deposition of an a-Si:H passivation layer. These interfacial modification techniques did not produce any significant improvement in the performance of solar cells with air exposed interfaces.

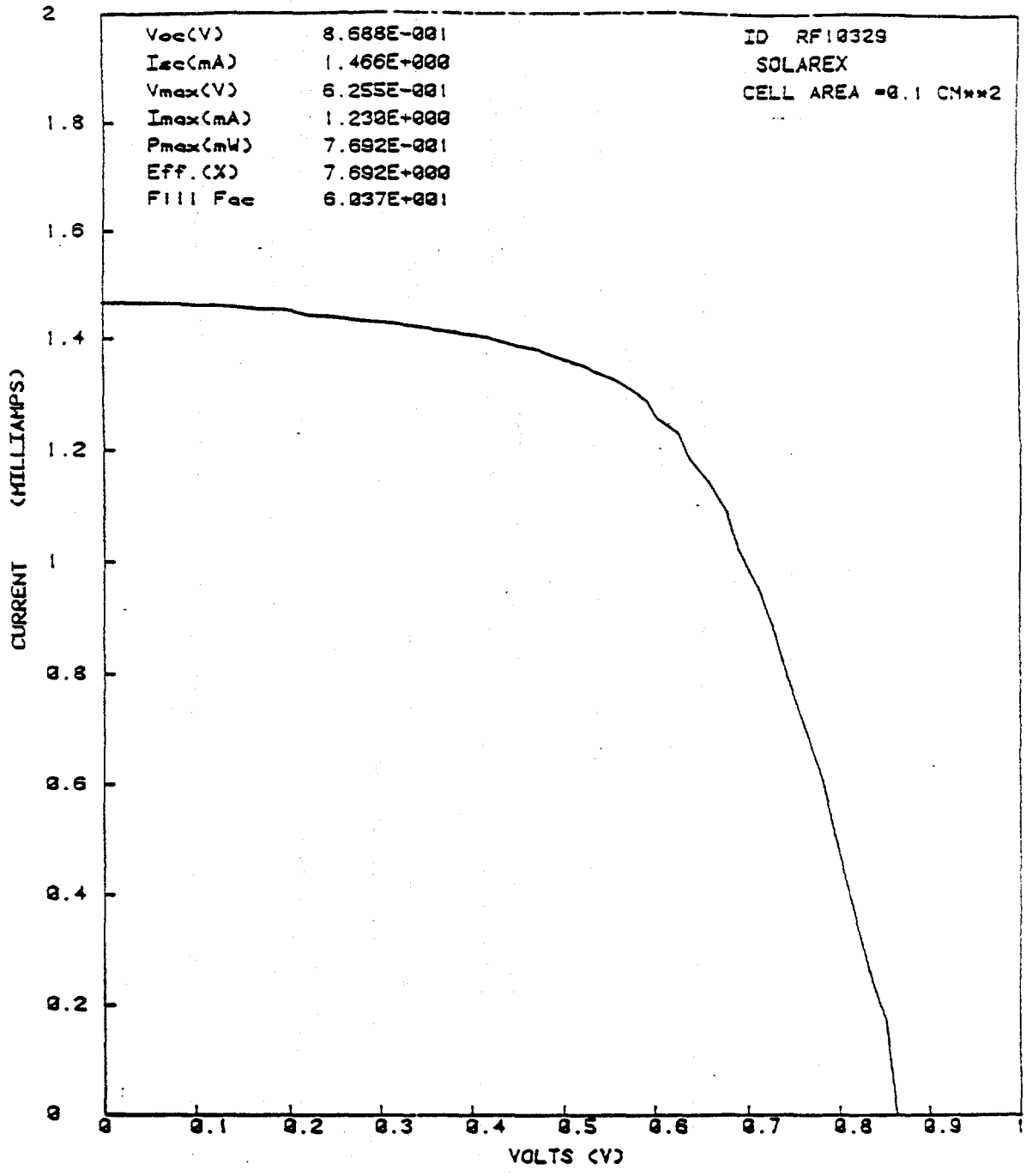

Figure 15. Improved Current-Voltage Characteristics of RF-Deposited, Base-line a-Si:H Solar Cells Using Solarex Substrates.

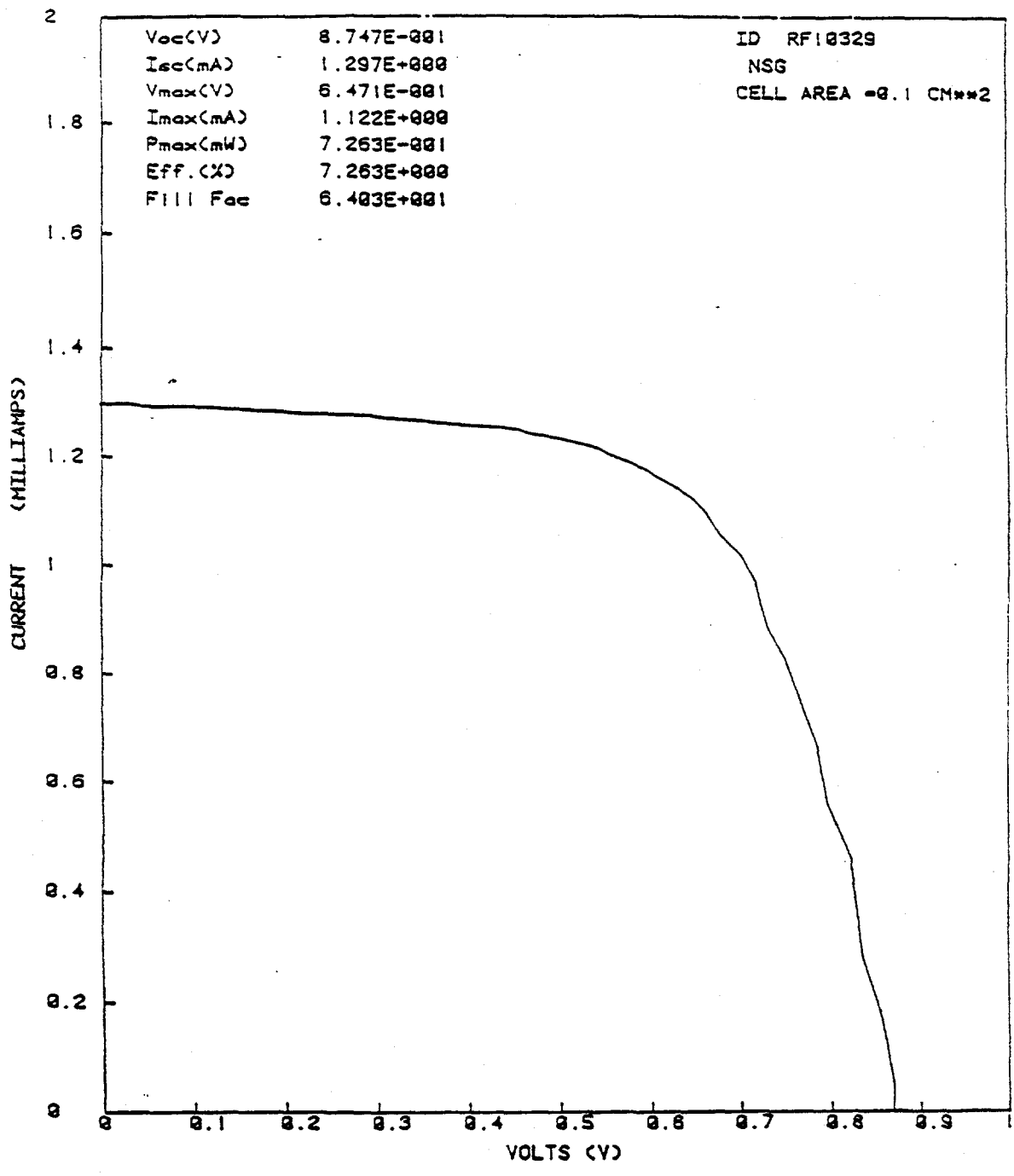

Figure 16. Improved Current-Voltage Charactgeristics of RF-Deposited, Base-line Solar Cells Using NSG Substrates.

4. ECR-Deposited a-Si:(Xe,H) Films Using Xenon Plasma Gas

We produced highly photosensitive a-Si:(Xe,H) films by ECR using xenon (Xe) as a plasma gas. The use of Xe plasma gas is an innovative approach for realizing the beneficial effects of low-energy ion bombardment. The high atomic mass of Xe produces a significant increase in the momentum of low-energy bombarding ions. We performed ECR depositions of a-Si:H films using pure Xe and mixed Xe/H_2 plasma gases and SiH_4 source gas.

We optimized the ECR deposition conditions of a-Si:(Xe,H) films, focusing upon gas flow rates, deposition pressure, substrate temperature, microwave power and magnetic field settings. Typical deposition conditions for ECR-deposited a-Si:H and a-Si:(Xe,H) films are shown in Table III. We deposited samples upon Corning 7059 glass, single-crystal Si wafers and high purity Al foil substrates. We selected these substrate materials for performing CPM, FTIR and SAXS measurements, respectively.

We measured the optical transmission of ECR-deposited a-Si:(Xe,H) films over the wavelength range of 0.5 to 2.0μm. We determined the index of refraction and the optical bandgap of this film by analyzing the optical transmission spectrum. Figure 17 shows the index of refraction of an ECR-deposited film as a function of the wavelength. The corresponding Tauc plot for determination of the optical bandgap is shown in Figure 18. The index of refraction decreased from about 4.0 at 0.5μm to about 3.3 at 2.0μm. The optical bandgap is 1.79 eV. These index of refraction values are higher than those of conventional ECR-deposited a-Si:H films, and the optical bandgap is lower than that of conventional ECR a-Si:H films. These optical characteristics indicate that Xe plasma deposited a-Si:(Xe,H) is a denser material, probably due to the reduced hydrogen content.

We performed light soaking experiments on a-Si:(Xe,H) films using concentrated AM 1.5 simulated solar illumination with a concentration ratio of about 7. We have previously shown that the equivalent, one sun, AM 1.5 illumination time of 80-100 hours is adequate for light soaking these films into a quasi-stabilized state for conductivity measurements. This can be expressed as:

$$\frac{\sigma_{ph}\ (t = \infty)}{\sigma_{ph}\ (t = 100\ hr)} \geq 0.9$$

Where σ_{ph} $(t = \infty)$ is the photocurrent after infinite illumination and σ_{ph} $(t = 100$ hr) is the photocurrent after 100 hr. illumination under 1-sun, AM 1.5 conditions.

Table III.

Deposition Conditions of JPL ECR-Deposited a-Si:H and a-Si(Xe,H) Films

Sample Number	Gas Flow Rates (sccm) SiH_4	H_4	Xe	Deposition Pressure (mTorr)	Substrate Temperature (°C)	Microwave Power Incident/ Reflected (W)	Magnetic Field Settings Top Coil/ Bottom Coil (W)
10716A	10	30	0	0.6	275	299/31	125/30
10717A	10	30	0	0.6	275	299/82	116/116
10717B	15	45	0	4	275	299/87	123/45
10719	15	45	0	4	250	299/96	123/45
10722A	15	45	0	5	250	299/92	123/45
10722B	40	40	0	5	250	299/85	124/40
20113A	20	40	15	3	350	299/60	114/135
20113B	20	40	15	3	350	299/50	135/135
20114A	20	40	15	3	400	300/55	113/135
20115A	20	40	15	3	350	300/64	113/135 H_2 Annealing
20115B	20	0	15	1	350	300/60	135/135
20116A	20	0	15	1	250	298/58	135/135
20116B	20	0	0	4	250	298/50	135/135

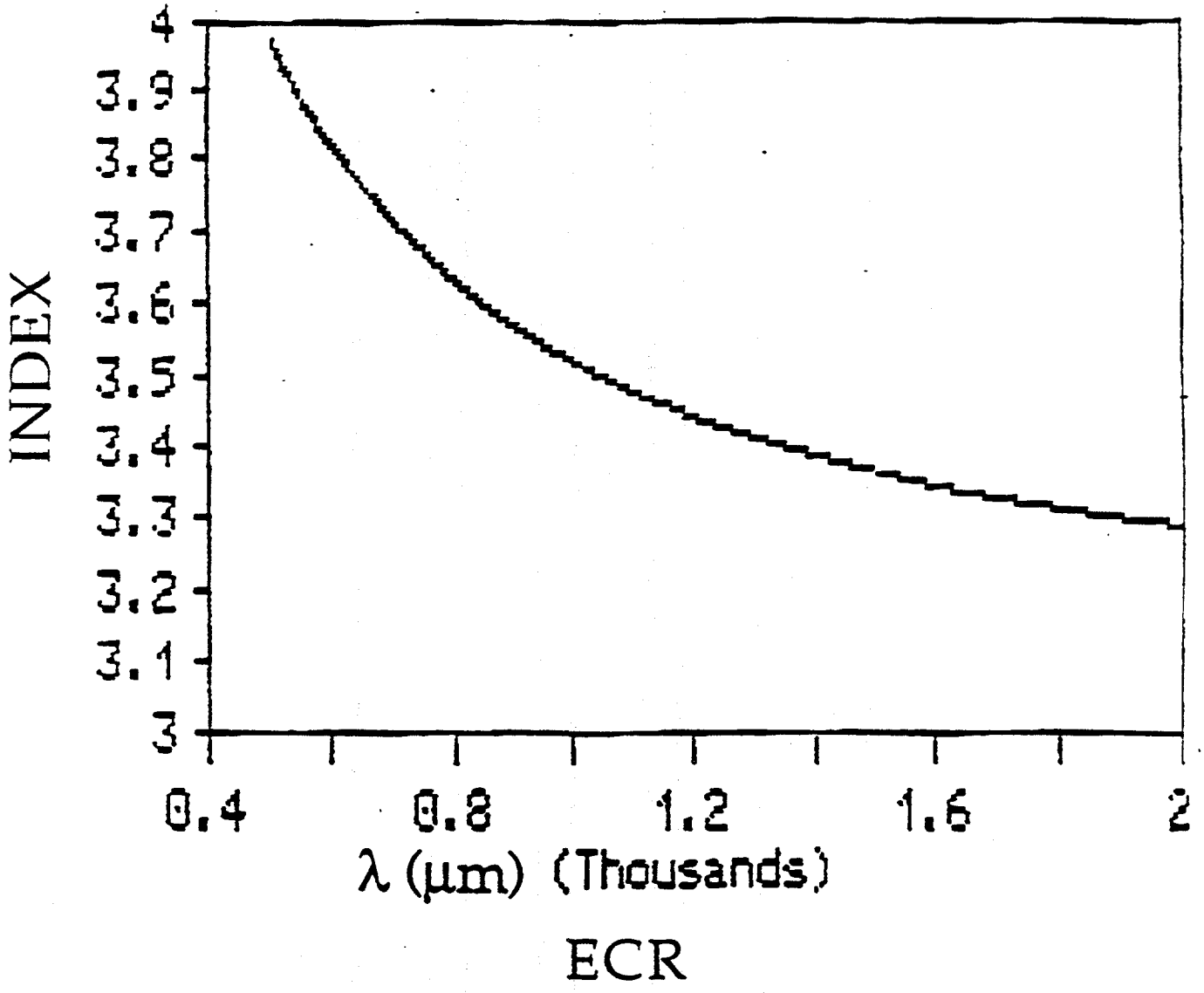

Figure 17. Index of Refraction for ECR-Deposited Film as a Function of Wavelength λ.

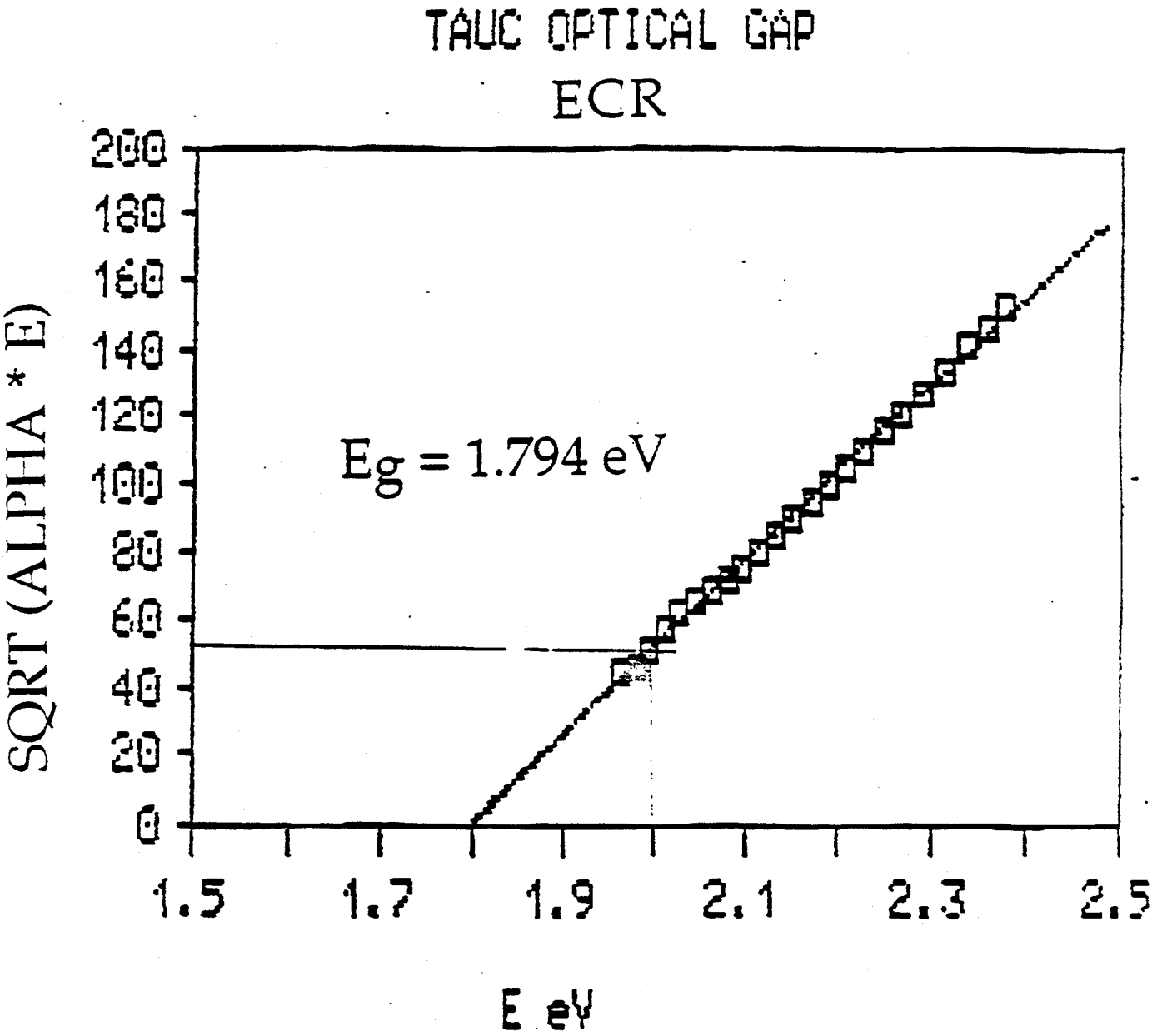

Figure 18. Tauc Plot for Sample Characterized in Figure 17. Optical bandgap is determined to be 1.79 eV.

Figure 19 shows light and dark conductivities of a-Si:(Xe,H) films and of a conventional RF-deposited a-Si:H film as a function of the illumination time. The light and dark conductivities of a-Si:(Xe,H) films with a high photosensitivity of 10^6 showed a reduced photodegradation rate, about 35% less than that of analogous RF-deposited a-Si:H films.

We performed constant photocurrent measurements (CPM) on highly photosensitive a-Si:(Xe,H) films. A typical CPM plot for a-Si:(Xe,H) films with photosensitivities of 10^6 is shown in Figure 20. We determined the characteristic slope of the Urbach exponential absorption tail of a-Si:(Xe,H) films to be 48 meV. A typical Tauc plot of a-Si:(Xe,H) films is shown in Figure 21; the optical bandgap is determined to be 1.72 eV. The material properties of ECR-deposited a-Si:(Xe,H), a-Si:H and RF-deposited a-Si:H films are summarized in Table IV, which shows that they have comparable material qualities, suitable for photovoltaic device applications. However, there is a significant improvement in photodegradation for ECR-deposited a-Si:(Xe,H) films, as shown by the initial-to-degraded light conductivity ratio.

The dark conductivity of 10^{-11} $(\Omega\text{-cm})^{-1}$ is low and stable, and is observed for the same films with high photosensitivities of 10^6. Certainly the dark conductivity is not related to either photostability or device stability. However, the photodegradation is directly related to the defect density of states in the material. This has a profound effect upon device performance. Without a stable i-layer, the device will, in turn, be unstable. Hence, this is one aspect of solar cell materials research and development which is relevant to examine prior to device growth.

In addition, the low, stable dark conductivity of 10^{-11} $(\Omega\text{-cm})^{-1}$ for a-Si:(Xe,H) films with a high photosensitivity of 10^6 is another indication of improved stability for device-quality materials.

We prepared special samples for small angle x-ray scattering (SAXS) measurements by depositing a-Si:(Xe,H) film onto high purity Al foils. We sent these samples to D. Williamson and S. Jones of the Colorado School of Mines for SAXS measurements.

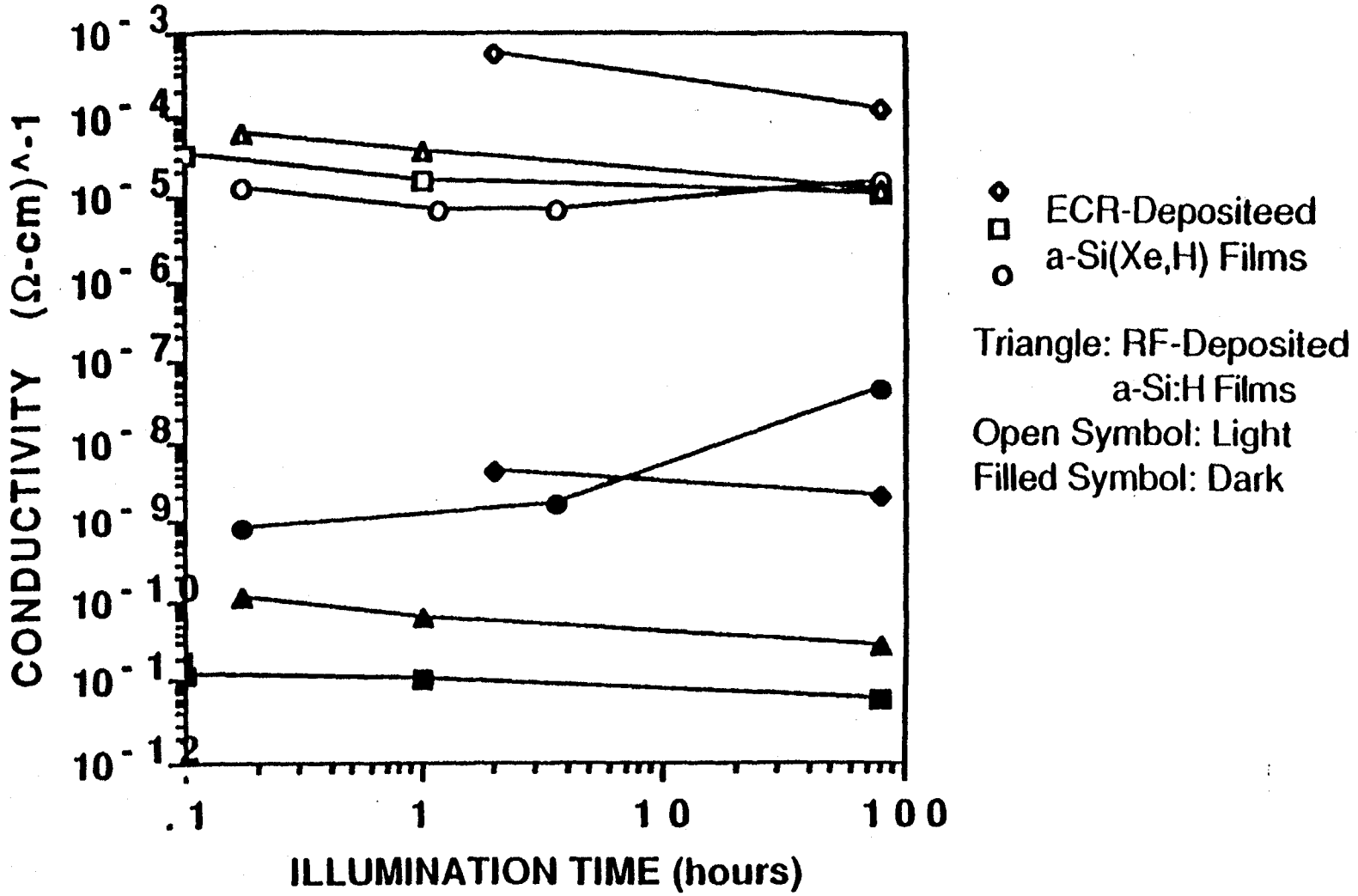

Figure 19. Light and Dark Conductivity a-Si:(Xe,H) Films as a Function of AM 1.5, 100 mW/cm^2 Illumination Time.

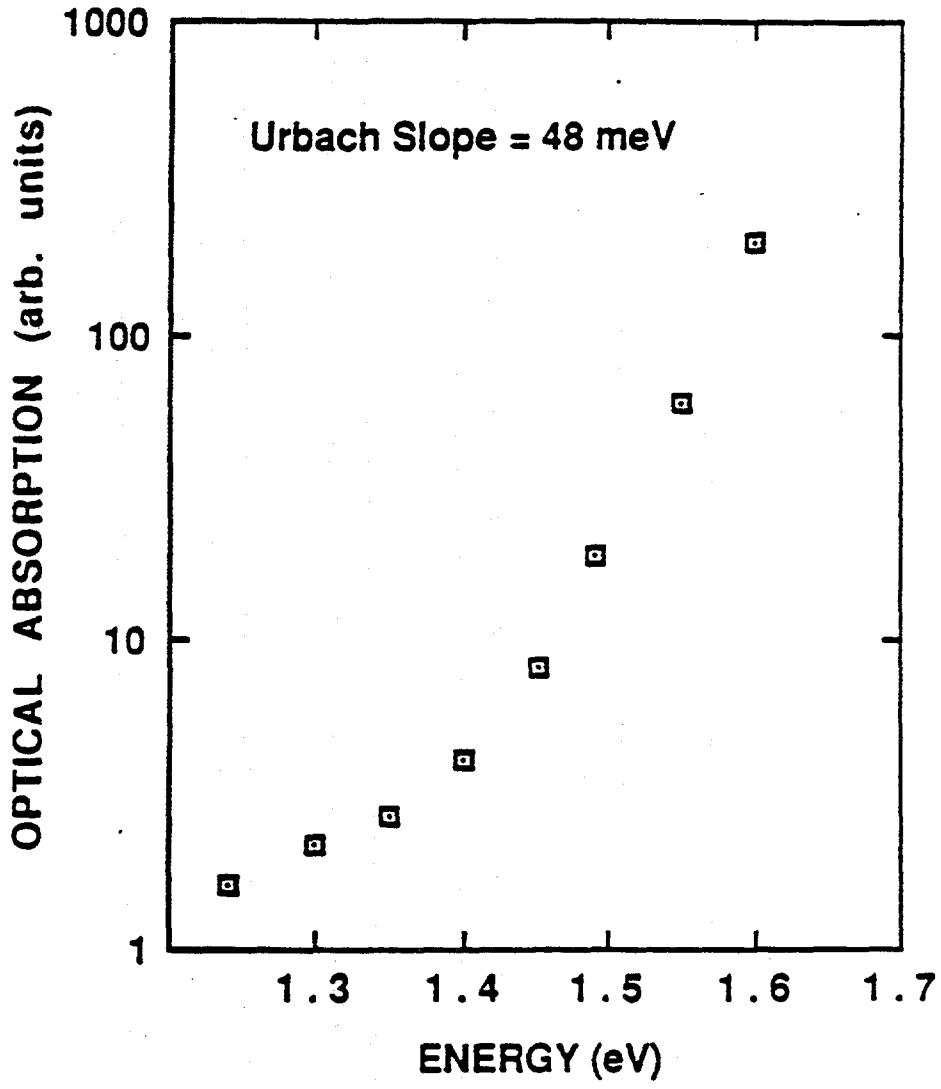

Figure 20. Typical Constant Photocurrent Measurements of a-Si:(Xe,H) Films with a Photosensitivity of 10^6.

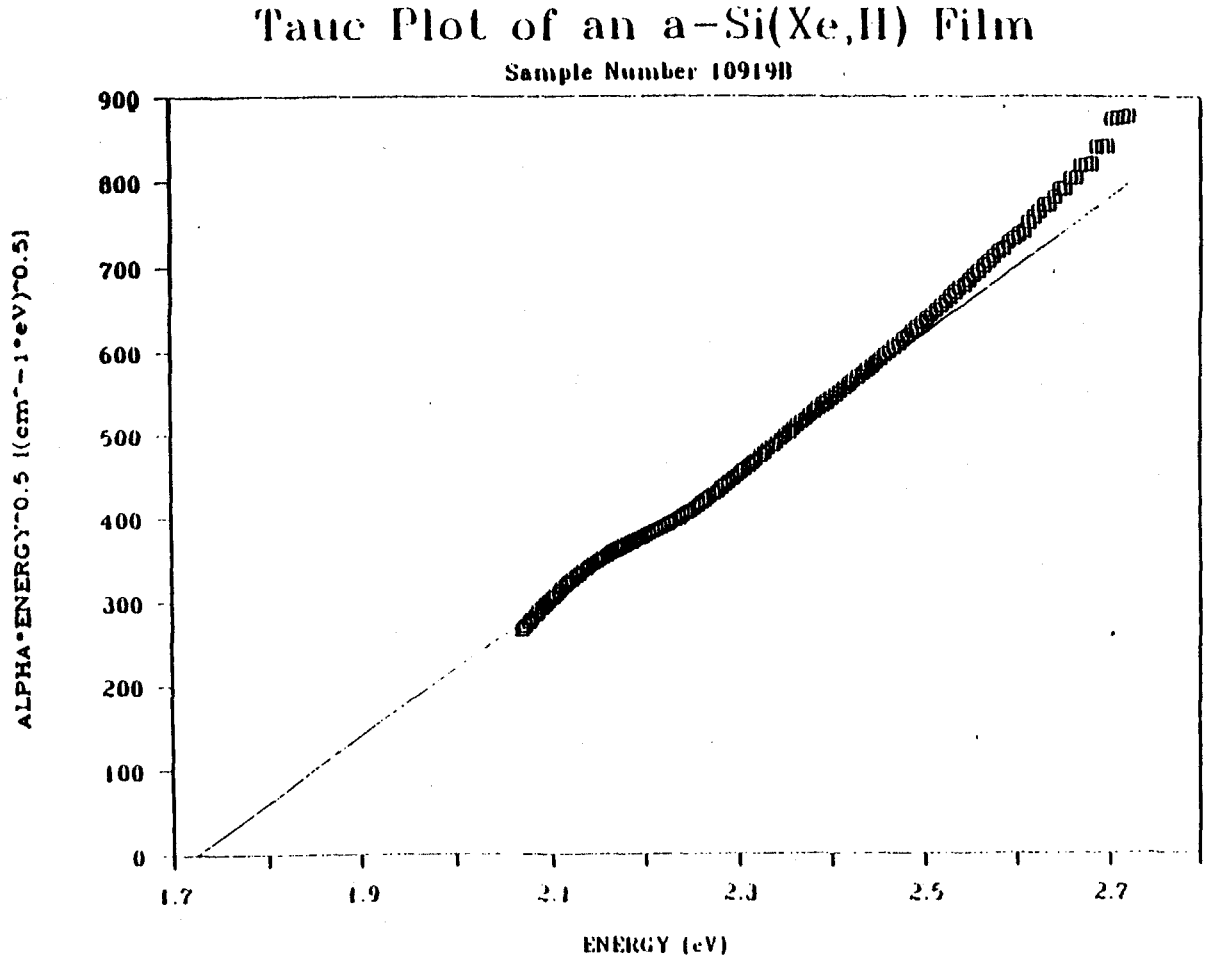

Figure 21. Tauc Plot of an a-Si:(Xe,H) Film Showing Optical Bandgap of 1.72 eV.

Table IV.

Material Properties of ECR-Deposited a-Si(Xe,H), a-Si:H and RF-Deposited a-Si:H Films

	ECR-Deposited a-SI(Xe,H)	ECR-Deposited a-Si:H	RF-Deposited a-Si:H
Initial Light Conductivity at 100 mW/cm^2 after 10 min. illumination: σ_L(10 min) $(\Omega\text{-cm})^{-1}$	2.9×10^{-5}	4.8×10^{-5}	6.0×10^{-5}
Degraded Light conductivity at 100 mW/cm^2 after 80 hours illumination: σ_L(80 hrs) $(\Omega\text{-cm})^{-1}$	1.1×10^{-5}	1.5×10^{-5}	1.4×10^{-5}
Dark conductivity σ_D $(\Omega\text{-cm})^{-1}$	1.2×10^{-11}	3.5×10^{-10}	1.2×10^{-10}
Initial Light-to-Dark Ratio: σ_L/σ_D	2.4×10^{6}	1.4×10^{5}	5.0×10^{5}
Initial-to-Degraded Light Conductivity Ratio: σ_L (10 min)/σ_L (80 hrs)	2.6	3.2	4.3
Urbach Slope: (meV)	48	50-60	55
Fermi Level: (eV)	--	0.85	0.8
Optical Gap: (eV)	1.72	1.80	1.73
Defect Density: (cm^{-3}) (Junction Capacitance Measurements)	--	$1\text{-}2 \times 10^{16}$	2×10^{16}

Figure 22 shows Guinier plots of JPL a-Si:(Xe,H) films where the natural log of the scattering intensity, I(h), is plotted as a function of $h=2\pi x$ (scattering angle/wavelength of the incident x-ray beam). The fraction of microvoids in the film, V_f, determined by SAXS, are as follows:

Sample Number	Microvoid Fraction V_f (%)
20113A	3.0
20114A	6.5
20115A	32.3
20115B	2.7
20116A	3.7
20116B	8.21

The typical microvoid fraction of ECR-deposited a-Si:(Xe,H) films is about 3%. This is quite close to the microvoid fraction (1-2%) of RF-deposited device-quality a-Si:H films. The large microvoid fraction of sample #20115A is attributed to the H_2 plasma annealing which altered the microstructure of the film. Sample 20114A was deposited at a high temperature of 400°C and sample #20116B was deposited without either H_2 or Xe plasma gas. Both these samples showed higher microvoid fractions (6-8%) than the typical value. The correlation between the microvoid fraction and the device performance has not yet been established and needs to be investigated.

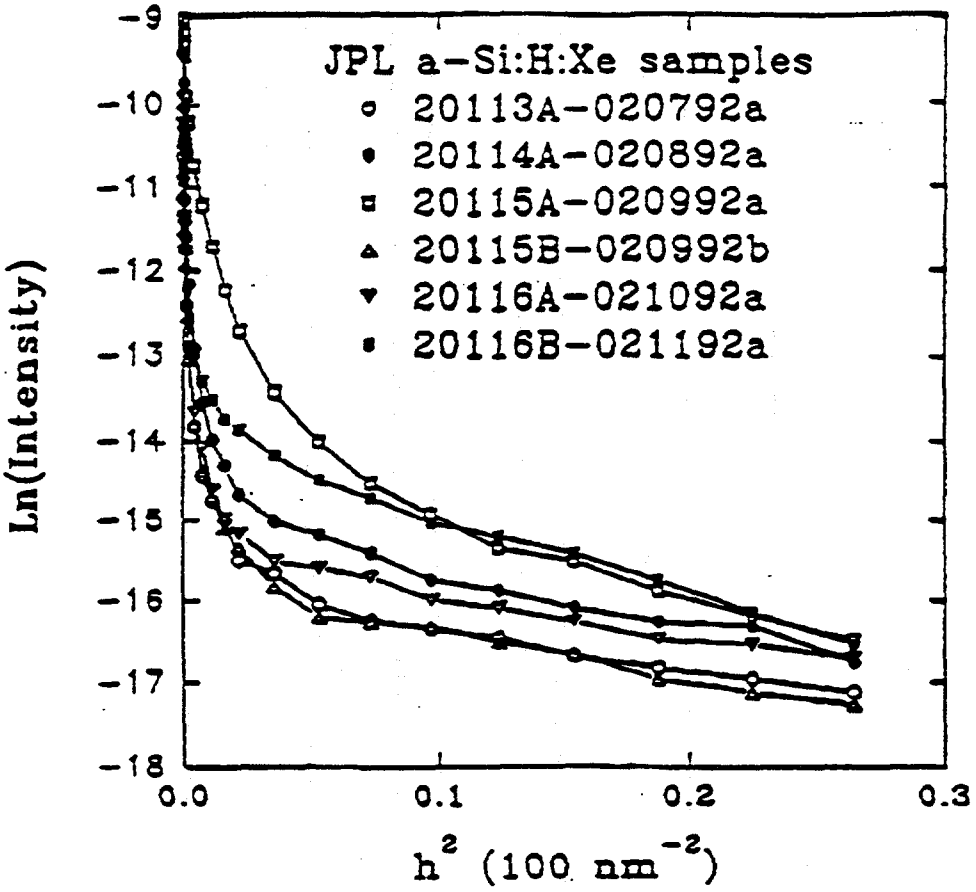

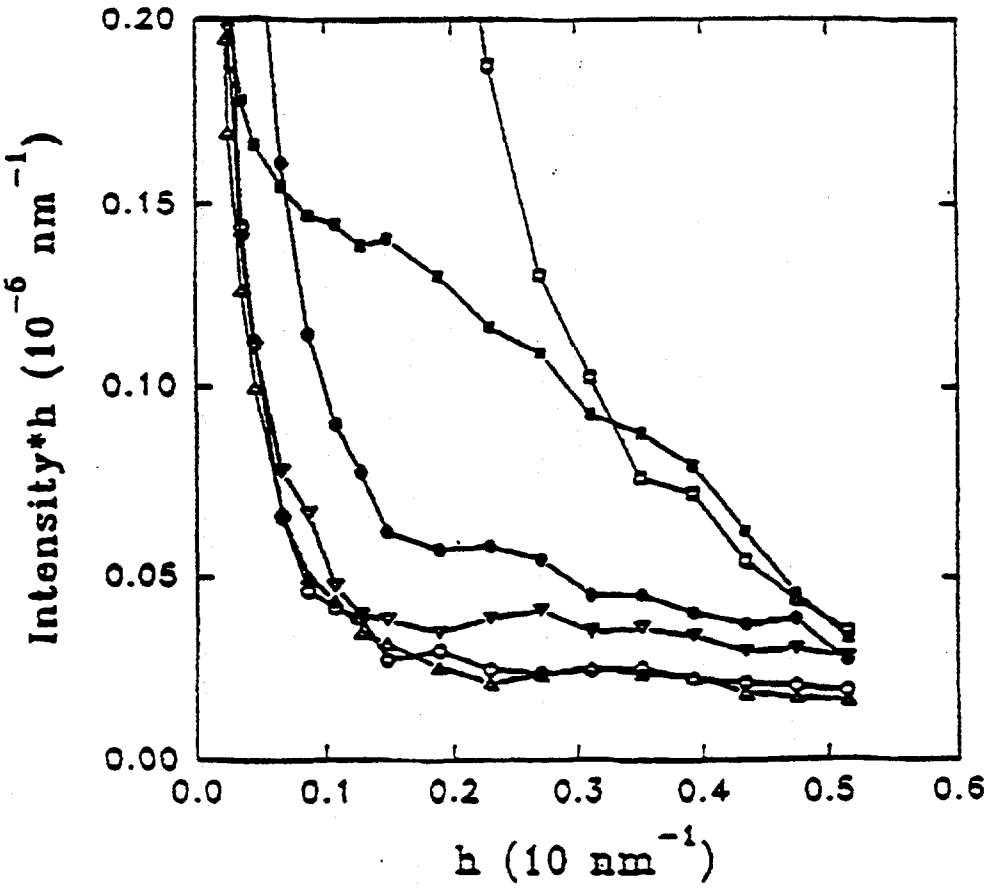

Figure 22. Guinier Plots of a-Si:(Xe,H) Films

5. Diagnostic Solar Cell Evaluation of ECR-Deposited a-Si:(Xe,H) Films

We fabricated diagnostic solar cells using RF-deposited p- and n-layers and ECR-deposited a-Si:(Xe,H) i-layers. The air exposure of the p/i and i/n interfaces has been a major limitation in optimizing the performance of the diagnostic solar cells. In future work, the insertion of an interlock between the ECR and RF chambers to eliminate interlayer air exposure is recommended.

The illuminated I-V characteristics of a diagnostic solar cell containing an ECR-deposited a-Si:(Xe,H) i-layer and air-exposed p/i and i/n interfaces is shown in Figure 23. The device performance of this diagnostic solar cell included a modest initial conversion efficiency of 4.1%, with an open-circuit voltage of 735 mV, a short-circuit current of 11.8 mA/cm^2 and a fill factor of 47%. In order to evaluate the device performance of a-Si:(Xe,H) films, a corresponding diagnostic solar cell containing all RF-deposited p, i and n layers and air-exposed p/i and i/n interfaces was also fabricated. Figure 24 shows the illuminated I-V characteristics of this RF-deposited diagnostic solar cell. Comparing Figures 23 and 24, the performance of the ECR-deposited a-Si:(Xe,H) film is comparable to that of the RF-deposited a-Si:H cell. The low conversion efficiency of both ECR- and RF-deposited diagnostic solar cells is attributed to the air exposure of the interfaces.

Light-soaking of both ECR and RF-deposited diagnostic solar cells was performed with concentrated, simulated AM 1.5 solar illumination at an intensity of 1 to 10 suns. The effective soaking time is determined by the experimentally observed scaling factor of intensity ratio to the power of 1.8. There is no measurable degradation in the device performance of both types diagnostic solar cells under an effective soaking time of up to about 500 hours. Table V shows the cell parameters as a function of the light soaking time for both RF and ECR-deposited i-layer diagnostic solar cells. The stable performance of these solar cells is probably the result of the already degraded performance due to the air exposure of the interfaces. However, the same performance of the ECR- and RF-deposited i-layer diagnostic solar cells indicate that the ECR-deposited a-Si:(Xe,H) films have at least the same material quality as that of the standard RF-deposited a-Si:H. Therefore, we conclude that the ECR-deposited a-Si:(Xe,H) is also of "device quality". This conclusion is corroborated if one examines the photoconductivity degradation of ECR and of RF glow discharge deposited material.

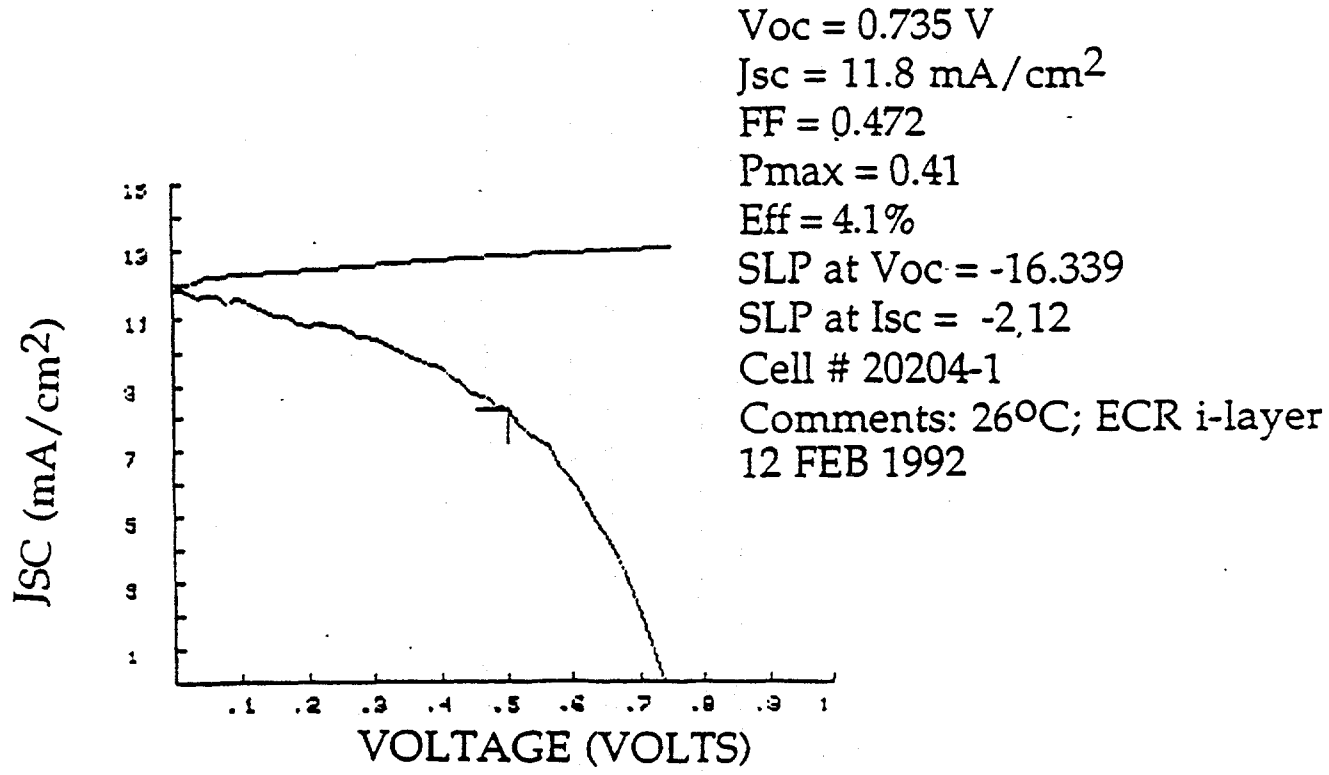

Figure 23. Illuminated I-V Characteristics of a Diagnostic Solar Cell Containing an ECR-Deposited a-Si:(Xe,H) i-layer

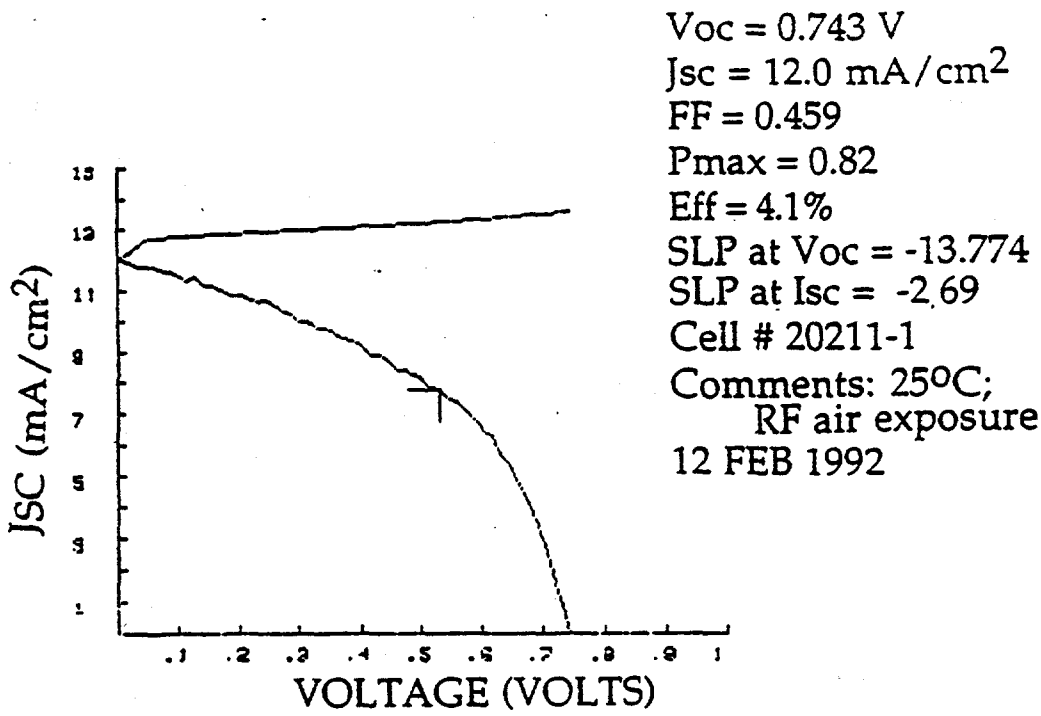

Figure 24. Illuminated I-V Characteristics of RF-Deposited Diagnostic Solar Cell

Table V. Light Soaking Characteristics for ECR- and RF- Deposited Solar Cell

LIGHT SOAKING

RF 20211

t (hr)	Voc (V)	Isc (mA/m^2)	EFF (%)	FF (%)
0	.75	10.8	3.78	45
3	.75	10.8	3.78	46
100	.75	10.4	3.64	47
233	.75	10.2	3.64	48
460	.75	10.2	3.64	48

ECR 20204

t (hr)	Voc (V)	Isc (mA/cm^2)	EFF (%)	FF (%)
0	.73	10.0	3.45	47
3	.73	10.1	3.43	48
108	.73	10.0	3.60	49
273	.73	10.0	3.67	51
508	.73	9.9	3.64	49

$$\text{time} = t \left(\frac{I}{Io} \right)^{1.8} \approx t\ (25)$$

a) Knox, Dalal and Popov reported the following data in the Journal of Vacuum Science and Technology:

$$\frac{\sigma_{pc}\ (t = 20\ hr)}{\sigma_{pc}\ (t = 0)} \quad \sim 1/16 \quad \text{for glow discharge films}$$

$$\frac{\sigma_{pc}\ (t = 20\ hr)}{\sigma_{pc}\ (t = 0)} \quad \sim 1/5 \quad \text{for thin ECR films}$$

Where σ_{pc} (t=20 hr) and σ_{pc} (t=0) are the photoconductivities after 20 and zero hours of light-soaking, respectively.

b) Johnson, et al. reported the following data in Applied Physics Letters:

The defect density (Ns) of glow-discharge a-Si:H increases by a factor of approximately five after 100 hours of AM 1.5 illumination. This corresponds to a photodegradation of approximately one order of magnitude. In comparison, JPL also finds (cf. Fig. 19 of this report) that:

$$\frac{\sigma_{pc}\ (t = 100\ hr)}{\sigma_{pc}\ (t \sim 0)} \quad \sim 1/5 \quad \text{for a-Si:(Xe,H)}$$

D. SUMMARY

Electron cyclotron resonance (ECR) microwave plasma-enhanced chemical deposition (PECVD) provides very desirable processing conditions for modifying film growth kinetics and for enhancing the surface reactions which promote growth at reduced substrate temperatures. The Jet Propulsion Laboratory developed a state-of-the-art ECR PECVD system for the deposition of a-Si:H and related alloy thin films.

The objective of this work was to obtain a fundamental understanding of amorphous silicon (a-Si:H) and related alloy thin film deposition processes by ECR microwave plasmas, with a best effort improvement of optoelectronic material properties and best effort photostabilization of solar cell performance.

We systematically and extensively investigated the ECR deposition parameter space for a-Si:H. The magnetic field profile and the selection of the plasma gas were found to play important roles in modifying the ECR deposition process via the control of the plasma density and ion energies.

The films underwent extensive materials characterization including: constant photocurrent measurement (CPM), to determine the Urbach slopes; junction capacitance measurements and drive-level capacitance profiling (DLCP), to determine the total integrated densities of filled defect states; optical transmission measurements, to determine the optical band gaps; light and dark photoconductivity measurements, to determine the photosensitivities; and small angle x-ray scattering (SAXS) measurements, to determine the microvoid fractions and distributions.

ECR-deposited, device-quality a-Si:H films showed typical light conductivities at 100 mW/cm^2 illumination of 5×10^{-5} $(\Omega\text{-cm})^{-1}$; photosensitivities of 1.4×10^5; Urbach slopes of 50-60 meV; and integrated defect densities of $1\text{-}2 \times 10^{16}$ cm^3. These material characteristics compare very favorably with standard values for RF-deposited a-Si:H films.

We also performed ECR deposition experiments on μc-Si:H; however, the material properties of μc-Si:H films could not meet the device requirements and hence, we did not pursue extensive characterization of these films.

We fabricated and tested diagnostic solar cells in order to provide device evaluations of the thin films. The ECR-deposited p-type a-SiC:H and intrinsic a-Si:H films, which were of primary interest to solar cells, underwent individual evaluation under device conditions, as components of p-i-n solar cells with standard RF films for the remaining layers. This required physical transfer of samples between the ECR and RF chambers, exposing the samples to air between layers and leading to some degradation of the inter-

faces. We obtained initial efficiencies as high as 5.9% for cells containing ECR p-type a-SiC:H windows, and initial efficiencies as high as 2.9% for cells containing ECR intrinsic layers. We emphasize that this low performance appears to be caused primarily to the interface degradation and does not appear to be related to ECR materials deficiencies. In support of this, RF-deposited cells with air exposure of the interfaces showed similarly low performance, from 7.7% for unexposed to 3.6% for exposed interfaces. Initial efficiencies of about 7.5% are regarded as state-of-the-art performance for a-Si:H solar cells which have not undergone supplementary optimization techniques. Also, light-soaked ECR a-Si:H shows an increase in defect density, evaluated by DLCP, which was comparable to that of analogous RF-deposited a-Si:H. In future work, insertion of an interlock between the two chambers would be one prospective solution to the air exposure problem.

Finally, we compared conventional ECR-deposited a-Si:H to a novel form of a-Si in which we added xenon gas to the ECR plasma during deposition. We investigated the ion bombardment effect as a function of the magnetic field profile. The large mass of the Xe atom effectively increases the momenta of the plasma ions. Indeed, initial characterization data of a-Si:(Xe,H) reveal that it is a very promising candidate material for producing cells with enhanced photostability. The new films processed low, stable dark conductivities and high photosensitivities. Light soaking experiments (e.g., 80 hours of AM 1.5 illumination at 100 mW/cm^2) revealed photodegradation rates which were about 35% less than those of comparable RF-deposited material. The reduced photo-degradation observed for ECR-grown a-Si:(Xe,H) material may eventually yield improved device photostability.

Photostability studies of intrinsic a-Si:H material are routinely discussed in the literature, including their relevance to eventual device performance. Although the preferred parameter of measurement is the creation of light-induced defects (Ns), the photoconductivity is directly related to Ns. Of course, actual device performance is ultimately required to determine the acceptability of a given material. However, initial studies of the material properties of the intrinsic a-Si:H layer are very relevant precursors.

Diagnostic solar cells containing a-Si:(Xe,H) i-layers, with air-exposed p/i and i/n interfaces, showed modest initial efficiencies of 4.1%. In perspective, a corresponding RF-deposited cell with air-exposed interfaces had an identical initial conversion efficiency of 4.1%. Again, this low performance appears to be caused primarily by the interface degradation and does not appear to be related to ECR materials deficiencies; in future work, insertion of an interlock between the two chambers would be one prospective solution of the air exposure problem.

JPL Proposal No. 80-3257A, submitted to the NREL on December 28, 1990, contained two milestones for the first year (months 1 through 12):

1. "Completely characterize and report on changes in RF-PECVD and ECR-PECVD intrinsic a-Si:H and μc-Si:H film properties before and after light-soaking the films under white light, approximately AM 1.5 and 100 mW/cm^2, as functions of ion bombardment and of resultant film properties." This milestone was fulfilled, as described above, particularly for a-Si:(Xe,H).

2. "Demonstrate the capability to fabricate diagnostic p-i-n solar cells using RF- a-Si:H intrinsic layers. These diagnostic p-i-n solar cells will become the baseline cells against which relative changes in the intrinsic layer material properties can be evaluated." This milestone was also fulfilled, as described above.

JPL not only performed the planned research, as shown by the completion of the two milestones, but also took initiative to investigate additional related research on a-Si:(Xe,H) to evaluate the ECR deposition technology for photovoltaic applications.

Further work on both ECR a-Si:H and a-Si:(Xe,H) could not proceed further under this task because of its termination. Although ECR material, particularly a-Si:(Xe,H) shows much promise in terms of materials photostability, we cannot yet make a solid assessment of device performance and photostability. In order to perform an adequate investigation on ECR-deposited a-Si:(Xe,) films, we suggest that material characterization experiments using FTIR, SAXS, CPM and light-soaking measurements should be continued and diagnostic solar cell fabrication incorporating a-Si:(Xe,H) films should be thoroughly investigated.

E. ACKNOWLEDGMENTS

This work was performed at the Center for Space Microelectronics Technology of the Jet Propulsion Laboratory. Dr. Yuh-Han Shing was the principal investigator and Task Manager. Dr. Frederick S. Pool was the co-investigator and provided technical contributions to the film deposition, characterization and device fabrication and testing. Dr. Carol Lewis, the Technical Group Supervisor, contributed to the technical planning and discussion of the task. Research collaborations with Dr. John Essick of Occidental College and Dr. Tom McMahon of NREL on CPM and junction capacitance measurements; with Dr. Scott Jones and Dr. Don Williamson of the Colorado School of Mines on SAXS measurements; and with Dr. John Webb of NREL on FTIR measurements are greatly appreciated. Finally, we thank Dr. A. Catalano of the Solarex Thin Film Division for providing SnO_2 coated glass substrates.

F. BIBLIOGRAPHY

1. S. Matsuo and M. Kiuchi, Jpn. J. Appl. Phys. 22, L210 (1983).

2. M. Matsuoka and K. Ono, Appl. Phys. Lett. 50, 1864 (1987).

3. M. Kitagawa, K. Setsune, Y. Manabe and T. Hirao, J. Appl. Phys. 61, 1084 (1987).

4. M. Matsuoka and K. Uno, T. Vac. Sci. Technol. Ab, 25 (1988).

5. S. Matsuo, Applied Solid State Science, Supplement 2C, Academic Press, New York, p. 75 (1785).

6. K. Kobayaski, M. Hayama, S. Kawamoto and H. Miki, Jpn. J. Appl. Phys. 26, 202 (1987).

7. H. Yamada and Y. Torii, Appl. Phys. Lett. 50, 386 (1987).

8. J. M. Essick, F. S. Pool, Y. H. Shing and M. J. Holboke, Mat. Res. Soc. Symp. Proc. 219, 679 (1991).

9. J. M. Essick, F. S. Pool and Y. H. Shing, J. Vac. Sci. Technol. A10, 521 (1992).

10. Y. H. Shing, F. S. Pool and J. M. Essick, Proc. 22nd Photovoltaic Specialists Conference, 1302 (1991).

11. R. D. Knox, V. L. Dalal and O. A. Popov, J. Vac. Sci. Technol., A9, 474 (1991).

12. N. M. Johnson, et al., Appl. Phys. Lett. 59, 1443 (1991).

Document Control Page	1. NREL Report No. NREL/TP-411-5123	2. NTIS Accession No. DE93000023	3. Recipient's Accession No.

4. Title and Subtitle

Electron Cyclotron Resonance Deposition of Amorphous Silicon Alloy Films and Devices

5. Publication Date

October 1992

6.

7. Author(s)

Y.-H. Shing

8. Performing Organization Rept. No.

9. Performing Organization Name and Address

Jet Propulsion Laboratory
Pasadena, California 91109

10. Project/Task/Work Unit No.

PV241101

11. Contract (C) or Grant (G) No.

(C) DD-1-11002-1

(G)

12. Sponsoring Organization Name and Address

National Renewable Energy Laboratory
1617 Cole Blvd.
Golden, CO 80401-3393

13. Type of Report & Period Covered

Technical Report
1 April 1991 - 31 March 1992

14.

15. Supplementary Notes

NREL technical monitor: W. Luft

16. Abstract (Limit: 200 words)

This report describes work to develop a state-of-the-art electron cyclotron resonance (ECR) plasma-enhanced chemical vapor deposition (PECVD) system. The objective was to understand the deposition processes of amorphous silicon (a-Si:H) and related alloys, with a best-effort improvement of optoelectronic material properties and best-effort stabilization of solar cell performance. ECR growth parameters were systematically and extensively investigated; materials characterization included constant photocurrent measurement (CPM), junction capacitance, drive-level capacitance profiling (DLCP), optical transmission, light and dark photoconductivity, and small-angle X-ray scattering (SAXS). Conventional ECR-deposited a-Si:H was compared to a new form, a-Si:(Xe,H), in which xenon gas was added to the ECR plasma. a-Si:(Xe,H) possessed low, stable dark conductivities and high photosensitivites. Light-soaking revealed photodegradation rates about 35% lower than those of comparable radio frequency (rf)-deposited material. ECR-deposited p-type a-SiC:H and intrinsic a-Si:H films underwent evaluation as components of p-i-n solar cells with standard rf films for the remaining layers.

17. Document Analysis

a. Descriptors

amorphous silicon ; films ; electronic devices ; deposition ; photovoltaics ; solar cells

b. Identifiers/Open-Ended Terms

c. UC Categories

271

18. Availability Statement

National Technical Information Service
U.S. Department of Commerce
5285 Port Royal Road
Springfield, VA 22161

19. No. of Pages

59

20. Price

A04

Form No. 0069E (6-30-87)